Elsevier Editorial System(tm) for Structure
Manuscript Draft

Manuscript Number: STRUCTURE-D-10-00047

Title: Systematic bioinformatics and experimental validation of yeast complexes reduces the rate of attrition during structural investigations

Article Type: Ways and Means

Keywords: Tandem affinity tag purification, high-throughput expression, multi-protein complexes; bioinformatics

Corresponding Author: Dr. Anastassis Perrakis, PhD

Corresponding Author's Institution: Netherlands Cancer Institute

First Author: Mark A Brooks, PhD

Order of Authors: Mark A Brooks, PhD; Kamil Gewartowski, PhD; Eirini Mitsiki, PhD; Juliette Létoquart; Roland A Pache; Ysaline Billier; Michela Bertero; Margot Corréa; Mariusz Czarnocki-Cieciura; Michal Dadlez; Véronique Henriot; Noureddine Lazar, PhD; Lila Delbos; Dorothée Lebert; Jan Piwowarski; Pascal Rochaix; Bettina Böttcher, PhD; Luis Serrano, PhD; Bertrand Séraphin, PhD; Herman van Tilbeurgh, PhD; Patrick Aloy, PhD; Anastassis Perrakis, PhD; Andrzej Dziembowski, PhD

Abstract: For high-throughput structural studies of protein complexes of composition inferred from proteomics data, it is crucial that candidate complexes are selected accurately. Herein, we exemplify a procedure that combines a bioinformatics tool for complex selection with an in vivo validation, to deliver structural results in a medium-throughout manner. We have selected a set of twenty yeast complexes, which were predicted to be feasible by either an automated bioinformatics algorithm, by manual inspection of primary data, or by literature searches. These complexes were validated with two straightforward and efficient biochemical assays, and heterologous expression technologies of complex components were then used to produce the complexes to assess their feasibility experimentally. Approximately one half of the selected complexes were useful for structural studies, and we detail one particular success story. Our results underscore the importance of accurate target selection and validation in avoiding transient, unstable, or simply non-existent complexes from the outset.

Suggested Reviewers: Shoshana Wodak PhD
Scientific Director, Centre for Computational Biology , Hospital for Sick Children, Toronto
shoshana@sickkids.ca
Dr. Wodak is an expert in the field of protein-protein interaction networks.

Aled M Edwards PhD
Professor, Banting and Best Dept of Medical Research, University of Toronto
aled.edwards@utoronto.ca
Dr Edwards is a highly knowledgeable member of the structural genomics community, and a pioneer in the field structural genomics, particularly with regards to protein complexes.

Mark B Gerstein PhD
Professor, Dept of Molecular Biophysics and Biochemistry, Yale University
Mark.Gerstein@Yale.edu

Dr. Gerstein is a renowned expert in the bioinformatic treatment of functional genomics and other information, for the purpose of predicting protein networks.

Tom S Peat PhD
Research Program Leader, Molecular & Health Technologies, CSIRO
Tom.Peat@csiro.au
Dr Peat is renowned for his expertise in structural genomics both at Los Alamos and SGX, prior to his present position.

Opposed Reviewers:

Cover Letter

Nederlands Kanker Instituut -
Antoni van Leeuwenhoek

Anastassis Perrakis
Group Leader
Netherlands Cancer Institute
Plesmanlaan 121
1066 CX Amsterdam
The Netherlands
20th February 2010

T + 31 20 512 1951
F + 31 20 512 1954
a.perrakis@nki.nl
http://xtal.nki.nl/

Dear Editors,

We would like to submit for your consideration our paper entitled: "Systematic bioinformatics and experimental validation of yeast complexes reduces the rate of attrition during structural investigations" for consideration as a "Ways and Means" article. This paper consolidates our experience on the use of large data sets, the yeast proteome - interactome, as the basis to for structural studies of protein complexes. Our results were obtained as part of a large European collaborative project, 3D-repertoire, which has brought together various laboratories with experience in systems biology, bioinformatics, structural biology and molecular biology, in an effort to provide new insight to the yeast proteome. A significant part of that effort was to provide new structural data of protein complexes, as the basis to promote our understanding of specific protein interactions in eukaryotic cells.

In this paper we exemplify a procedure combining bioinformatics tools for complex selection, *in vivo* validation and heterologous recombinant expression technologies, to deliver structural results in a medium-throughout manner. In addition, we showcase a test of twenty yeast complexes that were treated in this manner, and discuss in more detail one such complex that went all the way from identification to structural characterization.

To our knowledge this is the first time than an objective study has been done to evaluate the importance of bioinformatics analysis on pull down results to select the best possible targets for structural characterization. We believe this report is of broad interest to the molecular and structural biology communities, and that Structure is the ideal vehicle to bring our results to the attention of the broad readership that we wish to address.

The authors declare that they have no conflict of financial interest with the work presented herein.

Yours sincerely,

Anastassis Perrakis

Systematic bioinformatics and experimental validation of yeast complexes reduces the rate of attrition during structural investigations

Mark A. Brooks[1,†,‡], Kamil Gewartowski[2,‡], Eirini Mitsiki[3,‡], Juliette Létoquart[4], Roland A. Pache[5], Ysaline Billier[4], Michela Bertero[6], Margot Corréa[4], Mariusz Czarnocki-Cieciura[3], Michal Dadlez[2], Véronique Henriot[4], Noureddine Lazar[1], Lila Delbos[1], Dorothée Lebert[4], Jan Piwowarski[2], Pascal Rochaix[4], Bettina Böttcher[7], Luis Serrano[6,8], Bertrand Séraphin[4,*,□], Herman van Tilbeurgh[1,□], Patrick Aloy[5,8,□], Anastassis Perrakis[3,□], Andrzej Dziembowski[2,□]

[1]IBBMC-CNRS UMR8619, IFR 115, Bât. 430, Université Paris-Sud, 91405, Orsay, France.

[2]Department of Genetics and Biotechnology, Warsaw University & Institute of Biochemistry and Biophysics, Polish Academy of Sciences, Pawińskiego 5a, 02106 Warsaw, Poland

[3]Department of Biochemistry, The Netherlands Cancer Institute, Plesmanlaan 121, 1066 CX Amsterdam, The Netherlands.

[4]Equipe Labelisée La Ligue, CGM, CNRS UPR2167, Avenue de la Terrasse, 91198 Gif-sur-Yvette Cedex, France.

[5]Institute for Research in Biomedicine (IRB) and Barcelona Supercomputing Center (BSC). c/ Baldiri I Reixac 10-12, 08028 Barcelona, Spain.

[6]Systems Biology Laboratory, Centre for Genomic Regulation, Barcelona, Spain

[7]School of Biological Sciences, University of Edinburgh, King's Buildings, Mayfield Road, Edinburgh EH9 3JR, United Kingdom

[8]Institució Catalana de Recerca i Estudis Avançats (ICREA)

[†]Present Address: Evotec (UK) Ltd., 114 Milton Park, Abingdon, Oxon, OX14 4SA, UK.

*Present address: IGBMC, 1 rue Laurent Fries, BP10142, 67404 Illkirch, France

[‡]These authors contributed equally to the work

Corresponding authors:

Patrick Aloy patrick.aloy@irbbarcelona.org

Andrzej Dziembowski andrzejd@ibb.waw.pl

Anastassis Perrakis a.perrakis@nki.nl

Bertrand Séraphin seraphin@igbmc.fr

Herman van Tilbeurgh Herman.Van-Tilbeurgh@u-psud.fr

Running Title:

Protein complex validation for structural biology

Keywords:

Tandem affinity tag purification, high-throughput expression, multi-protein complexes, bioinformatics

Abstract

For high-throughput structural studies of protein complexes of composition inferred from proteomics data, it is crucial that candidate complexes are selected accurately. Herein, we exemplify a procedure that combines a bioinformatics tool for complex selection with *in vivo* validation, to deliver structural results in a medium-throughout manner. We have selected a set of twenty yeast complexes, which were predicted to be feasible by either an automated bioinformatics algorithm, by manual inspection of primary data, or by literature searches. These complexes were validated with two straightforward and efficient biochemical assays, and heterologous expression technologies of complex components were then used to produce the complexes to assess their feasibility experimentally. Approximately one half of the selected complexes were useful for structural studies, and we detail one particular success story. Our results underscore the importance of accurate target selection and validation in avoiding transient, unstable, or simply non-existent complexes from the outset.

Introduction

Numerous large-scale proteomics initiatives in the model organism *Saccharomyces cerevisiae* have been reported over the last few years, and have provided evidence for thousands of new protein interactions and supplied a wealth of information about the composition of macromolecular complexes (Gavin et al., 2006; Ho et al., 2002; Ito et al., 2001; Krogan et al., 2006; Tarassov et al., 2008; Uetz et al., 2000). Nevertheless, the characteristics of protein interaction networks *in vivo* have not yet been rigorously untangled for any organism, let alone the faithful budding yeast. Now that such protein interaction datasets are in the public domain, a gauntlet has been thrown down to the scientific community to provide tools for assimilating these data with a view to developing algorithms and experimental methodologies for predicting the composition of complexes with high accuracy, thereby facilitating their functional and structural characterization.

However, for many predicted complexes identified in high-throughput affinity purification experiments, their subunit composition is not established with sufficient reliability to proceed to structure determination. Improvements in the confidence that can be placed in protein interaction models are therefore clearly needed, with the specific aim of identifying complexes with well-defined stoichiometry, and which are amenable to structural studies. Raising the confidence with which complex composition could be predicted would benefit enormously the field of structural biology. Ideally, it would be possible to identify stable complexes (for example ribosomes, RNA polymerases, the exosome, or the 20S proteosome) and discriminate them from more dynamic assemblies that contain transient interactors (for example spliceosomes or the 26S proteosome). It would therefore be beneficial to classify and characterize the various entities which form the central frameworks of protein-protein interaction networks (Gavin et al., 2006; Higurashi et al., 2008; Krogan et al., 2006).

Foremost among the problems encountered in complex characterization are those related to the primary data being of limited quality. For example, the heterogeneity or the extremely dilute nature of samples from proteomic experiments results in complex subunits being overlooked. Additionally, in some studies, the characterization of complex composition has been hindered by the contamination of *bona fide* complexes by so-called ‘background’ or ‘sticky’ polypeptides that interact

with other proteins in a promiscuous fashion (Shevchenko et al., 2002). One challenge is therefore to devise a computational strategy to filter through the results of many thousands of biochemical purifications which have been performed to date, and identify the complexes that will yield the optimal results during expression and purification studies (Bravo and Aloy, 2006).

The first structural genomics consortia focused on the determination of X-ray and NMR structures at the level of the single protein (Alzari et al., 2006; Graslund et al., 2008; Marsden and Orengo, 2008). More recently, the Structural Genomics Consortium (SGC)(Edwards et al., 2002), the 3D Repertoire (http://www.3drepertoire.org/) and SPINE 2 - Complexes (http://www.spine2.eu/) consortia have opted to study macromolecular complexes from a medium-throughput perspective. The expression and purification of protein complexes adds an extra level of complexity, since globular protein interfaces are often partly hydrophobic, and single partners may be insoluble. In many cases, only in the context of an assembled complex do hydrophobic interfaces become buried and the participating polypeptides can be produced as soluble entities (Dyson and Wright, 2005; Smialowski et al., 2007).

Since the inception of the European Commission-funded consortium “3D repertoire” in 2004, collaborating scientists have been addressing the problems associated with identifying complexes *de novo* for structural studies. Within the first step, which consisted of highly selective filtering of existing datasets for evidence of the existence of complexes in a process we term ‘complex triage’, three methods were employed. Firstly, a bioinformatics-based selection procedure, optimized using a training set composed of complexes of known three-dimensional (3D) structure, was used to screen for stable, well-folded complexes. Secondly, we examined the results from high throughput affinity purification experiments manually, focusing on the visual inspection of gels to identify complexes of which the components existed in stoichiometric quantities. Finally, a set of seven complexes was chosen on the basis of the scientific literature.

A compilation of these complexes, named the 'list of 20', were then validated by new affinity purifications of the natural complexes and their subunit compositions were confirmed using mass spectrometry. In addition, the solution sizes of these complexes were assessed by size exclusion chromatography. The subset of proteins

that were shown to indeed participate in macromolecular assemblies as predicted and that was also believed to be tractable for structural studies was then cloned and expressed in *E. coli*. Using various techniques, we aimed to obtain purified material suitable for structural analysis. We show the overall success in each of the steps of this procedure and present a detailed account of one example complex. The results from this test set of complexes under investigation have allowed us to evaluate the effectiveness of each of the techniques used and devise an optimal route for the production of protein complexes in structural biology pipelines.

Results

Identification of complexes for structural studies

Complex triage by bioinformatics

A system has been previously described for the ranking of the 491 complexes and the 5,488 isoforms that we had previously described from over 2,000 successful tandem affinity purifications (Gavin et al., 2006). This was based on the notion that target complexes likely amenable to structural studies should be small, compact and homogeneous. We considered biophysical, biochemical and large-scale proteomics data in the form of partial scoring functions that were normalized and combined into a final feasibility score for each complex (c.f. Methods, Supplemental Methods, and as described previously (Pache and Aloy, 2008); referred to hereafter as the Complex Feasibility (CF) algorithm). In this way, the public domain data were filtered to generate a much-reduced subset of credible complexes. To generate a list of a total of seven complexes by the CF tool, we combined four of the top ranking choices with three mid-ranking complexes (Table 1, Table S3).

Complex triage by manual visualization of gels

In the original genome-wide approach (Gavin et al., 2006), tandem affinity purified (TAP) assemblies were separated by denaturing gel electrophoresis and stained. The gels were then cut into 1 mm slices, digested with trypsin and analyzed by MALDI–TOF mass spectrometry (MS). However, this procedure did not take into account the relative quantities of proteins present in the TAP eluate. Complexes with apparent sub-stoichiometric components are more likely to depend on labile transient interactions and less suitable for structural studies than stable stoichiometric assemblies. We thus decided to visually inspect the original gels (Gavin et al., 2006) for bands indicative of stoichiometric complexes. The resulting assemblies were narrowed down to dimers, trimers and tetramers. Thorough inspection of about 4,000 purification experiments, we identified 64 promising complexes (Table S4; dimeric complexes, Table S5; trimeric complexes, Table S6; tetrameric complexes). Not all of the 64 chosen complexes were present in the computational selection, simply because some of these were not identified as being complexes in the original automated

annotation (Gavin et al., 2006). Notably, the best six complexes that were chosen independently by gel inspection were all in the top-50 of the CF algorithm, and two of them were in the top-10. Six complexes were finally selected by manual gel inspection (Table 1).

The list of '20 complexes'

In Table 1, we show the 20 complexes selected, with the corresponding bioinformatics and gel scores, and when possible appropriate references to the literature. Although the manual gel inspection and the bioinformatics efforts were independent, all previously identified complexes selected by manual screening had a high ranking using the CF algorithm. In contrast, not all of the complexes chosen by the algorithm could be associated with clear and conclusive gels. Notably, a top-ranked choice was associated with a gel of mediocre quality. Nonetheless, such types of selections resulted in a potentially interesting collection of complexes that would hopefully be amenable to structural studies. The selection was complemented by the choice of an additional seven complexes suggested by partners of 3D repertoire, based on specific biological interests and literature know-how, reaching the final number of 20 complexes included in this study. Interestingly, only one of the latter choices was in the top-10 bioinformatics list, and an additional two were in the top-50; the remaining four scored poorly by the CF algorithm.

Validation of complex composition

The twenty selected complexes were validated in a two-step TAP purification on IgG and calmodulin columns. Mass spectrometry analyses using an ESI-TRAP approach were performed using both the eluate solutions and the excised gel bands as samples. In addition, molecular weights of complexes were estimated by size exclusion chromatography of total extracts, followed by dot-blot detection of TAP-tagged proteins in eluate fractions. Finally, the molecular weights of tagged subunits and the efficiency of binding to IgG resin were verified by Western blot analyses (see Figure 1 for a schematic representation of the procedure). The conclusions regarding individual complexes are presented in Table 1 and Figure S1.

Only two of the complexes completely failed this validation stage, one for technical reasons and one could not be identified at all. Interestingly, both complexes originated from the literature additions to the list and they both scored poorly in the

bioinformatics assessment. This category, where literature knowledge was used to select complexes, gave a lower validation rate than the other strategies. Apart from the one complex for which no technically valid results were obtained, one failed, while two others showed too weak native expression to be conclusive. Another complex was highly heterogeneous and one included a very promiscuous protein as a partner and was thus inconclusive. Notably, one complex selected from the literature and validated here to be 'excellent', was ranked in the top-10 (20^{th} percentile) of the bioinformatics list. The low validation rates of complexes selected from the literature, and their low bio-computing ranks stem from their specific characteristics (low abundance, specific interaction involving abundant partners flagged as promiscuous) and underline the limitation of current strategies to identify *bona fide* complexes. The gel-selected complexes and the bioinformatics complexes fared well in the validation, with four out of six and three out of seven, respectively, being scored as 'excellent'. From the validated complexes, eleven were chosen for heterologous expression studies and production in quantities suitable for structural studies. Analysis of the twelfth complex, Dom34:Hbs1 is described elsewhere, so was not repeated (Graille et al., 2008), but is included in Table 1.

Recombinant production of complexes for structural studies

For these eleven complexes, a mixture of expression strategies was employed for their evaluation: expression of the full-length individual subunits, *in vitro* complex reconstitution from subunits, and co-expression. A total of twenty-two proteins have been used in expression trials as single full-length proteins in *E. coli*, either from synthetic, codon-optimized genes (16 proteins, Figure 2, panel A) or from natural yeast genes (Figures S2, S3, S4, S5 and S6). Only three of these failed to produce soluble protein in appreciable amounts (Atg29, Psy4 and Ste11). We proceeded to reconstitute three complexes (Vps27:Hse1, Ptc2:Paa1 and Gcd10:Gcd14) from individually purified partners and succeeded in purifying them in soluble form and defined subunit composition. In parallel, we also attempted co-expression of nine complexes, and we were able to produce seven out of nine complexes by such co-expression methods, (Figure 2, panel B).

A case study of an example complex, from selection to validation

To illustrate the course of an experiment from target selection to validation, we present one particular exemplary complex. The Gcd10:Gcd14 complex was originally identified a few years ago and purified as a dimeric tRNA(1-methyladenosine) methyltransferase (Anderson et al., 1998; Anderson et al., 2000; Ozanick et al., 2007). Gavin et al. (Gavin et al., 2006) observed again this dimeric complex, which was annotated as Complex 376 in the Krogan et al. enumeration (Krogan et al., 2006). TAP purified Gcd10:Gcd14 has also been shown to be relatively homogeneous and therefore pure by electron microscopy. We selected this complex by gel analysis but it also ranked with a score of 12 by the CF algorithm.

Firstly, we re-validated the complex by repeating the TAP purification using tagged Gcd14 and the only partner that was isolated was Gcd10, with no other bands either apparent or identified by mass spectrometry Figure 3, panels A and B). Gel filtration analysis of the TAP-tag purified complex was consistent with a molecular weight of approximately 350 kDa, suggesting the formation of higher-order multimers since the expected mass of the Gcd10:Gcd14 complex with a 1:1 stoichiometry is 98.3 kDa.

The complex was reconstituted from the Ni^{2+}-NTA purified individual components and subjected to gel filtration chromatography. The resulting complex had an approximate molecular weight of around 350 kDa, in agreement with the analysis of the 'native' TAP-tagged complex (Figure 3, panel B). The purified complex was then used in a negative stain electron microscopy experiment. The sample was homogeneous and could be used for data collection (Figure 3, panel C). Image reconstructions without any imposed symmetry showed a tetrameric core with extensions at opposite surfaces, giving the entire complex two-fold, as well as quasi four-fold symmetry. Therefore, C2-symmetry was imposed for further refinement. The final reconstruction is shown in Figure 3, panel E. Projections of this reconstruction agree with class averages were determined by multivariate statistical analysis (Figure 3, panel D).

Discussion

In this work, we set out to identify an optimal strategy for the analysis of *Saccharomyces cerevisiae* complexes by combining contemporary structural biology tools with the numerous proteome-level biochemical interaction datasets. Our central tenet was that we believed such data to be essentially reliable, the use of improved bioinformatics tools, manual analysis of gels or bibliographic curation of previous data should allow the identification of complexes best suited to structural analysis.

A question that we sought to answer related to whether bioinformatics, and specifically the CF algorithm, could provide trustworthy guidance when selecting targets. Ideally, the algorithm should eliminate the need for manual inspection of data. Therefore, we first generated a target list, partly using automated tools and partly manually. The next step was to ascertain which of the selected complexes do indeed exist in a stable and stoichiometric form. Our experimental results show that the bioinformatics algorithm could select targets with a validation success rate that was very high, and comparable to visual inspection of gels.

In the final CF algorithm, the most important parameters were the yeast two-hybrid ratio and the socio-affinity index (Table S2). The usefulness of the former parameter has been obvious for some time, since yeast two-hybrid screening has been a mainstay of research into protein-protein interactions. However, the important role of the socio-affinity index in this experiment was encouraging (Gavin et al., 2006), and we believe that it is a valuable and powerful metric for the identification of protein complexes based on protein interaction datasets. Conversely, the least useful parameters were the 'average number of problematic residues' and the 'co-localization ratio'; it appears that these parameters are not as useful as had been previously thought, at least in the context of this work (Pache and Aloy, 2008).

We note that some complexes identified by bibliographic analyses, which could not be validated and for which low scores were obtained with the CF algorithm, performed well using recombinant expression. These facts underline the limitation of complex analyses of low abundance complexes and/or complexes involving very abundant subunits for which it is difficult to exclude the existence of promiscuous interactions. It is possible that our complex triage procedures have been successful at

least in part, due to the clarity of primary data for which the subunits are stoichiometrically equivalent and well expressed.

The success rate of obtaining soluble subunits by heterlogous recombinant expression, for the full-length proteins was high (only 3 of 22 proteins tested could not be produced in a soluble form; 86% success rate). Similarly, we were able to obtain soluble complexes corresponding to most of our validated targets using either complex reassembly or co-expression *via* either co-transformation of plasmids or single plasmids that contain operons encoding all of the proteins of interest (c.f. Table 1, and Supplemental Material; 9 of 11 complexes could be formed; 82% success rate). We believe that this achievement is principally due to the efficient selection criteria that we had established. It has been reported that only about 20% of full-length eukaryotic proteins are soluble when produced in a heterologous expression system (Graslund et al., 2008), but the performance of our approach is considerably superior. This is likely to be because only natively soluble proteins and complexes that are expressed at suitably high levels are detected by mass spectrometry after TAP purification, thereby biasing complex identification data towards soluble proteins.

Based on the four-year experience of a consortium of numerous structural biology groups involved in 3D repertoire, we suggest an optimal experimental strategy for the high-throughput study of protein complexes. We conclude that despite the absence of a 'silver bullet', much can be achieved first by triaging the targets by an efficient computational procedure, followed by simple expression and reconstitution in the first instance. For this, a LIC-based strategy to clone optimized synthetic genes in a parallel manner resulted in notable success, with 14 of 16 subunits expressed in soluble form. During complex reconstitution, we had greater success when employing co-sonication of *E. coli* in which each subunit had been expressed separately, compared to reconstitution using pure proteins and has become our method of choice to obtain soluble complexes (c.f. Supplemental Experimental Procedures; 'Complex formation trials').

We also found that producing plasmids that encode the necessary subunits as synthetic DNA, with Shine-Dalgarno sequences upstream of the successive ORFs to be a very practical and rapid method of co-expressing complexes (c.f. Supplemental

Experimental Procedures; ‘Cloning strategy used for poly-cistronic expression’). Our studies into the use of polycistronic vectors, particularly those constructed from synthetic genes (*e.g.* Gcd10:Gcd14 and Ssl2:Yor352 complexes, Figure S8) indicate that this is a strategy that this is a useful addition to pipelines, both because of the ease of production of plasmid constructs, and the increase in yield presented by codon-optimized genes.

In summary, we conclude that when initiating projects involving high-throughput study of protein complexes, proper triaging and validation is obligatory. Once this had been performed, it was relatively straightforward to test the association of the recombinant proteins experimentally. As we illustrate with the Gcd10:Gcd14 complex, we were able to obtain structural information during the relatively short time scale of this project. In this work, we have leveraged complementary strategies to the end of complex production for structural analysis, but we envisage the incorporation of further techniques in subsequent experiments. For example, high throughput small angle X-ray scattering studies of single proteins could be applied similarly to complexes (Hura et al., 2009), and it will be increasingly important to identify complex and sub-complex composition of samples purified directly from cells using native mass spectrometry (Hernandez et al., 2006). Accurate subunit prediction and validation methods will be beneficial to future high-throughput approaches geared towards ‘high-hanging fruit’ and increase the probability that such efforts will yield illuminating insights into macromolecular machines at work.

Acknowledgements

This work was supported in part by the European Union 6th Framework program “3D-repertoire” (LSHG-CT-2005-512028) to HvT, AP, PA, LS and to BS. An EMBO young investigator award supported AD. We thank Claire Batisse (EMBL Heidelberg) for technical assistance in electron microscopy. The authors declare that they have no conflict of financial interest with the work presented herein. LS, PA and BS conceived of the study and MB coordinated the work between the contributing laboratories. PA and RAP performed the bioinformatics analysis. KG and AD performed the in-vivo validation. EM and MC-C carried out the expression and coexpression testing using single plasmids and synthetic genes. MAB, NL, LD worked on expression and *in vitro* reconstitution of complexes. JL, YB, MC, VH, DL and PR worked on complex production through various co-expression methods. NL and MAB produced and characterized the Gcd10:Gcd14 and BB performed electron microscopy on it. BS, HvT, AP and AD supervised the work in their laboratories. MAB and AP and wrote the article, with contributions from MB, LS, BS, HvT, PA and AD.

Figure Legends

Figure 1: Strategy for the validation of selected complexes

A schema showing the overall pathway for the validation of complex composition and estimation of molecular weight of each complex is presented. The complexes were expressed in yeast using a C-terminal TAP-tag of the bait protein. Following cell-breakage, complexes were either subjected to TAP purification to assess the subunit composition, or to gel filtration in order to estimate the molecular weight, and thereby their stoichiometry. See Figure S1 for actual results of the validation experiments.

Figure 2: Expression and purification of yeast full-length proteins

Panel A: SDS-PAGE analysis of full-length yeast constructs produced using codon-optimized synthetic genes, Ni^{2+}-NTA-purified and visualised using Coomassie. Full-length proteins were expressed and purified as above and eluted material was analysed by SDS-PAGE. The samples are relatively pure after only one step of purification, although degradation products are sometimes present. Molecular weight markers and their sizes are indicated on both sides of the gel. Successful constructs are: Atg17 (48.7 kDa), Dug2 (98.1 kDa), Dug3 (40.2 kDa), Gcd10 (54.4 kDa), Gcd14 (43.9 kDa), Met12 (73.9 kDa), Met13 (68.6 kDa), Psy2 (98.1 kDa), Rbg2 (41 kDa), Gir2 (31 kDa), Ssl2 (95.3 kDa), Yor352w (39.3 kDa), Vps27 (71.9 kDa), Hse1 (51.1 kDa), while the unsuccessful constructs are: Atg20 (72.5 kDa) and Psy4 (50.7 kDa). Panel B: The nine complexes successfully produced in a recombinant form. Ni^{2+}-NTA-purified samples of the results of complex formation trials were subjected to SDS-PAGE analysis and visualised using Coomassie. Co-expressed or reconstituted forms of the Gcd10:Gcd14 (54.4 and 43.9 kDa, respectively), Paa1:Ptc2 (21.9 and 50.3 kDa), Met12:Met13 (73.9 and 68.6 kDa), Dug2:Dug3 (98 and 40.2 kDa), Ssl2:Yor352w (95.2 and 40.2 kDa), Hbs1:Dom34 (68.7 and 44.1 kDa), Vps27:Hse1 (71.9 and 51.1 kDa), Gir2:Rbg2 (31 and 41 kDa), Dug2:Dug3 (98.1 and 40.2 kDa), Rps28B:Edc3 (7.6 and 61.3 kDa) complexes. Bands corresponding to the proteins of interest are arrowed. See also Figure S2 for detailed results of expression and reconstitution of complexes.

Figure 3: Validation and scale-up of an exemplary complex; Gcd10:Gcd14

A) Both Gcd10 and Gcd14 were clearly visible after purification using the TAP protocol, with little evidence of contaminating proteins, validating this complex. B) In order to estimate the size of the complexes, yeast extracts were separated with the use of size exclusion chromatography on a Superdex 200 column in low (150 mM; marked as 'LO') and high (500 mM; 'HI') concentration of NaCl. 30 fractions from this chromatography step were collected and spotted on a nitrocellulose membrane. To detect fractions containing the TAP tagged protein, western blotting using PAP antibodies was performed. See the legend to Figure S1 for further details to panels A and B. C) Micrograph of the Gcd10:Gcd14 complex which had been purified as in Figure 2, panel B, and fixed with glutaraldehyde, according to the GraFix protocols (Kästner et al., 2008) and stained with uranyl-acetate in a sandwich between two layers of carbon. The length of the scale bar equals 50 nm. D) Class averages of the data (top row) determined by multi-statistical analysis agree with projections of the 3D-map (central row). Surface presentations (bottom row) of the 3D-map are shown in the same directions as the projections above. The length of the scale bar equals 5 nm. E) Image reconstruction of the Gcd10/Gcd14 complex. C2 symmetry was imposed during the final rounds of refinement. The complex is shown along the symmetry axis (left) and perpendicular to the symmetry axis (right). The length of the scale bar equals 5 nm.

Tables

Table 1: *Summary of target selection, validation and complex reconstitution results. Complexes selected by bioinformatics, gel and literature analyses respectively, are listed. The complexes were assessed according to their purity after TAP purification (column labeled "Gel quality"). The ranks according to the CF algorithm of each of the complexes ("Rank"), as well as the results of validation by tandem affinity purification (c.f. Figure S1; "TAP Validation" and Figure S2 for the results of complex production and Table S7) are shown. Results of expression, co-expression and reconstitution studies are as follows: +; successful, -; unsuccessful, ND; not determined, NA; not applicable. *; Few of the complexes consist of 3 or more subunits. [¥]The Gcd10:Gcd14 complex was not reconstituted from purified proteins, but instead cells in which the proteins had been expressed separately were combined prior to sonication. For clarity, results that were deemed to be 'positive' (having a 'good' gel quality, high ranking in the bioinformatics triage, significant expression levels or production of the relevant complex by either co-expression or by reconstitution) are shown with a green background. Similarly, 'mediocre' results in the TAP validation (indicating that either heterogenous or partial complexes were purified) are shown with a yellow background. Negative results, indicating either a poor gel quality, low bioinformatics rank, failed TAP validation experiment, failed expression or failed complex production, are shown in red. Expression results for the complexes not deemed to be suitable for structural analysis are shown as gray text. [‡]Reconstitution of the Dom34:Hbs1 complex is described previously (Graille et al., 2008).*

Stage / Complex	Selection		Validation	Single subunit expression		Complex production		
	Gel Quality	Rank	TAP Results	Subunit 1	Subunit 2	Re-constitution[¥]	Separate plasmid co-expression	Operon co-expression
Bioinformatics Analysis								
Ste11, Ste50	Good	1	Heterogeneous	+	-	-	ND	ND
Atg17, Atg20, Atg29	Good	27	Partial (Atg29 missing)	+	-	ND	-	-
Vps27, Hse1	Excellent	1	Excellent	+	+	+	+	ND
Psy2, Psy4, Pph3	Excellent	4	Partial (Pph3 missing)	+	-	ND	-	ND
Nup82, Nup159, Nsp1	Good	4	Excellent	ND	ND	ND	ND	ND
Ede1, Syp1	Good	22	Excellent	ND	ND	ND	ND	ND
Dop1, Mon2	Excellent	25	Aggregated	ND	ND	ND	ND	ND
Gel Analysis								
Gcd14, Gcd10	Excellent	12	Excellent	+	+	+	+	+
Ptc2, Paa1	Excellent	8	Paa1 promiscuous	+	+	+	ND	ND
Met12, Met13	Excellent	22	Excellent	+	+	ND	+	ND
Dug3, Dug2	Excellent	9	Excellent	+	+	ND	+	ND
Ssl2, Yor352w	Excellent	27	Excellent	+	+	ND	+	+
Spt6, Spn1	Excellent	40	Partial (Spn1 missing)	ND	ND	ND	ND	ND
Literature Analysis								
Rad17, Mec3, Dcd1	Failed	261	Failed	ND	ND	ND	ND	ND
Orc1-6	Good	29	Heterogeneous	ND	ND	ND	ND	ND
Rbg2, Gir2	Good	5	Excellent	+	+	ND	+	+
Dom34, Hbs1[‡]	No Interaction	364	No Interaction	+	+	+	ND	ND
Rps28B, Edc3	No Interaction	364	Edc3 promiscuous	ND	ND	ND	+	+
Sis2, Ykl088w, Vhs3	Partial Interaction	323	Weak expression	ND	ND	ND	ND	ND
Mtw1, Dsn1, Nnf1, Nsl1	Partial Interaction	11	Weak expression	ND	ND	ND	ND	ND

Methods

Validation

TAP purification

TAP tagged strains of *Saccharomyces cerevisiae* were grown in 4 l of YPD medium (1% yeast extract, 1% bacto-peptone, 2% glucose) to an optical density (O.D.) of approximately 2. Yeast pellets were resuspended in 40 ml of lysis buffer (1 mM DTT, 40 mM Hepes pH 8, 250 mM NaCl) and frozen in liquid nitrogen. Cells were broken in a laboratory blender cooled with dry ice. Extracts were defrosted with protease inhibitors and spun in 35Ti rotor (Beckman) in a Beckman ultracentrifuge at 20,000 rpm for 20 minutes at 4°C. Supernatant was spun again at 32,000 rpm for 90 minutes at 4°C. Resulting extracts were dialyzed in buffer D (1 mM DTT, 40 mM Hepes pH 8, 150 mM NaCl, 1 mM PMSF) and frozen in liquid nitrogen. Extracts were then defrosted and incubated with 200 μl of IgG Sepharose 6 Fast Flow resin (GE Healthcare) in the presence of 0.1% rTX-100 for 1.5 hours at 4^{o}C. The beads were washed twice with 10 ml IPP150 (10 mM Tris-HCl pH 8.0, 150 mM NaCl, 0.1% rTX100) and twice with 10 ml TEV cleavage buffer (10 mM Tris-HCl pH 8.0, 150 mM NaCl, 0.5mM EDTA, 1 mM DTT). TEV cleavage was performed for 2 hours using 20 μg of TEV protease in 300 μl of cleavage buffer at room temperature. Eluates were agitated with 300 μl of calmodulin beads suspension (Stratagene) for 0.5 hours at 4^{o}C. The beads were washed four times with 500 µl of calmodulin wash buffer (10 mM Tris-HCl pH 8.0, 150 mM NaCl, 10 mM β-mercaptoethanol, 1mM $CaCl_2$) and the protein was eluted with 0.6 ml calmodulin elution buffer (10 mM Tris-HCl pH 8.0, 500 mM NaCl, 10 mM β-mercaptoethanol, 0.1% rTX100, 4mM EDTA). As a control, denatured elution fractions from both IgG and calmodulin beads were prepared with 250µl of 1% SDS at 60^{o}C.

Protein precipitation and analysis by mass spectrometry

Proteins were precipitated using pyrogallol red(Aguilar et al., 1999). When salinity of buffer was higher then 200 mM of NaCl the samples were first adjusted to this concentration by dilution. Proteins were separated by electrophoresis performed on NuPAGE 4-12% gradient gels using MES buffer gel system (Invitrogen) and

stained with SimplyBlue SafeStain (Invitrogen). Mass spectrometry was performed both with IgG eluates in solution and from bands cut from gels. Samples were then processed by standard procedures with trypsin digestion and cysteine alkylation. The obtained peptide mixtures were separated on a nano-HPLC system and the column outlet was coupled to the ion source of an LTQ FTICR spectrometer.

Western blot analyses

After dialysis, extracts and flow-throughs after IgG Sepharose chromatography were separated by 10% SDS-PAGE and electro-blotted onto the Protran nitrocellulose membrane (Bioscience) using a Trans-Blot® system (Bio-Rad). The filters were blocked for 1 h in 5% milk powder in PBS containing 0.1% Tween-20 and then the mouse monoclonal anti-rabbit immunoglobulin–peroxidase conjugate (Sigma) diluted 3,000-fold was added. After one hour, the blots were washed three times in PBS with 0.1% Tween-20. Finally, horseradish peroxidase conjugates were visualized by enhanced chemi-luminescence system (ECL, GE Healthcare).

Mass determination of the complexes

In order to estimate the size of the purified complex the extract from TAP-tagged strains was separated according to size, by size exclusion chromatography on a Superdex 200 10/300 column (GE Healthcare) using an Akta Purifier FPLC. Two different salt concentrations (150 mM and 500 mM NaCl) were used for elution and fractions were collected into a 96 well plate. 60 μl of every fraction were spotted on a nitrocellulose membrane. TAP tagged subunits were detected by Dot-Blot as described for western blot analyses. The intensities of the spots were calculated with ImageQuant (GE Healthcare) and exported into chromatograms. The column was calibrated using protein markers; thyroglobulin (670 kDa), ferritin (440 kDa), catalase (232 kDa), aldolase (154 kDa), albumin (67 kDa), ovalbumin (43 kDa) and chymotrypsin (25 kDa).

Electron Microscopy and Image Processing

The purified, over-expressed Gcd10/Gcd14 complex was fixed on a glycerol gradient with glutaraldehyde according to the GraFix protocol(Kästner et al., 2008). Fractions of the gradient were further analyzed by dot-blot analysis using an antibody against the 6-histidine tag. The dot blot identified a single peak with a maximum at

fraction 14. Samples from the peak fractions were prepared for subsequent electron microscopy by sandwich negative stain using uranyl acetate as previously described(Ulbrich et al., 2009). Samples were imaged at room temperature in a Philips CM120 Biotwin electron microscope at 100 kV. Data was recorded on a 4kx4k Tietz-CCD camera at a nominal pixel size of 4.27 Å per pixel under low dose conditions. For further processing 10819 particle images were selected from 29 micrographs. Three-dimensional models were calculated using sinogram correlation and weighted back projection with IMAGIC 5(van Heel et al., 1996). The process of determining initial orientations followed by calculation of a three-dimensional map was repeated several times using different class averages for starting the sinogram correlation.

Projections of the resulting three-dimensional models were compared with the initial class averages. The model that generated projections that matched most of the initial class averages, was selected for further refinement by an iterative process of projection matching followed by calculating a new 3D-map with Spider(Frank et al., 1996). After five rounds of refinement the map was stable and showed an approximately fourfold-symmetric core with extensions at opposite sides, giving the whole map a 2-fold symmetric appearance. Therefore, the map was refined for another five rounds imposing C2-symmetry. The resolution of the final map was determined by Fourier-Shell-Correlation and was 23 Å (Correlation=0.5).

References

Aguilar, R.M., Bustamante, J.J., Hernandez, P.G., Martinez, A.O., and Haro, L.S. (1999). Precipitation of dilute chromatographic samples (ng/ml) containing interfering substances for SDS-PAGE. Anal Biochem *267*, 344-350.

Alzari, P.M., Berglund, H., Berrow, N.S., Blagova, E., Busso, D., Cambillau, C., Campanacci, V., Christodoulou, E., Eiler, S., Fogg, M.J., *et al.* (2006). Implementation of semi-automated cloning and prokaryotic expression screening: the impact of SPINE. Acta Crystallogr D Biol Crystallogr *62*, 1103-1113.

Anderson, J., Phan, L., Cuesta, R., Carlson, B.A., Pak, M., Asano, K., Bjork, G.R., Tamame, M., and Hinnebusch, A.G. (1998). The essential Gcd10p-Gcd14p nuclear complex is required for 1-methyladenosine modification and maturation of initiator methionyl-tRNA. Genes Dev *12*, 3650-3662.

Anderson, J., Phan, L., and Hinnebusch, A.G. (2000). The Gcd10p/Gcd14p complex is the essential two-subunit tRNA(1-methyladenosine) methyltransferase of Saccharomyces cerevisiae. Proc Natl Acad Sci U S A *97*, 5173-5178.

Bravo, J., and Aloy, P. (2006). Target selection for complex structural genomics. Curr Opin Struct Biol *16*, 385-392.

Dyson, H.J., and Wright, P.E. (2005). Intrinsically unstructured proteins and their functions. Nat Rev Mol Cell Biol *6*, 197-208.

Edwards, A.M., Kus, B., Jansen, R., Greenbaum, D., Greenblatt, J., and Gerstein, M. (2002). Bridging structural biology and genomics: assessing protein interaction data with known complexes. Trends Genet *18*, 529-536.

Frank, J., Radermacher, M., Penczek, P., Zhu, J., Li, Y., Ladjadj, M., and Leith, A. (1996). SPIDER and WEB: processing and visualization of images in 3D electron microscopy and related fields. J Struct Biol *116*, 190-199.

Gavin, A.C., Aloy, P., Grandi, P., Krause, R., Boesche, M., Marzioch, M., Rau, C., Jensen, L.J., Bastuck, S., Dumpelfeld, B., *et al.* (2006). Proteome survey reveals modularity of the yeast cell machinery. Nature *440*, 631-636.

Graille, M., Chaillet, M., and van Tilbeurgh, H. (2008). Structure of yeast Dom34: a protein related to translation termination factor Erf1 and involved in No-Go decay. J Biol Chem *283*, 7145-7154.

Graslund, S., Nordlund, P., Weigelt, J., Hallberg, B.M., Bray, J., Gileadi, O., Knapp, S., Oppermann, U., Arrowsmith, C., Hui, R., *et al.* (2008). Protein production and purification. Nat Methods *5*, 135-146.

Hernandez, H., Dziembowski, A., Taverner, T., Seraphin, B., and Robinson, C.V. (2006). Subunit architecture of multimeric complexes isolated directly from cells. EMBO Rep *7*, 605-610.

Higurashi, M., Ishida, T., and Kinoshita, K. (2008). Identification of transient hub proteins and the possible structural basis for their multiple interactions. Protein Sci *17*, 72-78.

Ho, Y., Gruhler, A., Heilbut, A., Bader, G.D., Moore, L., Adams, S.L., Millar, A., Taylor, P., Bennett, K., Boutilier, K., *et al.* (2002). Systematic identification of

protein complexes in Saccharomyces cerevisiae by mass spectrometry. Nature *415*, 180-183.

Hura, G.L., Menon, A.L., Hammel, M., Rambo, R.P., Poole, F.L., 2nd, Tsutakawa, S.E., Jenney, F.E., Jr., Classen, S., Frankel, K.A., Hopkins, R.C., *et al.* (2009). Robust, high-throughput solution structural analyses by small angle X-ray scattering (SAXS). Nat Methods *6*, 606-612.

Ito, T., Chiba, T., Ozawa, R., Yoshida, M., Hattori, M., and Sakaki, Y. (2001). A comprehensive two-hybrid analysis to explore the yeast protein interactome. Proc Natl Acad Sci U S A *98*, 4569-4574.

Kästner, B., Fischer, N., Golas, M.M., Sander, B., Dube, P., Boehringer, D., Hartmuth, K., Deckert, J., Hauer, F., Wolf, E., *et al.* (2008). GraFix: sample preparation for single-particle electron cryomicroscopy. Nat Methods *5*, 53-55.

Krogan, N.J., Cagney, G., Yu, H., Zhong, G., Guo, X., Ignatchenko, A., Li, J., Pu, S., Datta, N., Tikuisis, A.P., *et al.* (2006). Global landscape of protein complexes in the yeast Saccharomyces cerevisiae. Nature *440*, 637-643.

Marsden, R.L., and Orengo, C.A. (2008). Target selection for structural genomics: an overview. Methods Mol Biol *426*, 3-25.

Ozanick, S.G., Bujnicki, J.M., Sem, D.S., and Anderson, J.T. (2007). Conserved amino acids in each subunit of the heteroligomeric tRNA m1A58 Mtase from Saccharomyces cerevisiae contribute to tRNA binding. Nucleic Acids Res *35*, 6808-6819.

Pache, R.A., and Aloy, P. (2008). Incorporating high-throughput proteomics experiments into structural biology pipelines: identification of the low-hanging fruits. Proteomics *8*, 1959-1964.

Shevchenko, A., Schaft, D., Roguev, A., Pijnappel, W.W., and Stewart, A.F. (2002). Deciphering protein complexes and protein interaction networks by tandem affinity purification and mass spectrometry: analytical perspective. Mol Cell Proteomics *1*, 204-212.

Smialowski, P., Martin-Galiano, A.J., Mikolajka, A., Girschick, T., Holak, T.A., and Frishman, D. (2007). Protein solubility: sequence based prediction and experimental verification. Bioinformatics *23*, 2536-2542.

Tarassov, K., Messier, V., Landry, C.R., Radinovic, S., Serna Molina, M.M., Shames, I., Malitskaya, Y., Vogel, J., Bussey, H., and Michnick, S.W. (2008). An in vivo map of the yeast protein interactome. Science *320*, 1465-1470.

Uetz, P., Giot, L., Cagney, G., Mansfield, T.A., Judson, R.S., Knight, J.R., Lockshon, D., Narayan, V., Srinivasan, M., Pochart, P., *et al.* (2000). A comprehensive analysis of protein-protein interactions in Saccharomyces cerevisiae. Nature *403*, 623-627.

Ulbrich, C., Diepholz, M., Bassler, J., Kressler, D., Pertschy, B., Galani, K., Bottcher, B., and Hurt, E. (2009). Mechanochemical removal of ribosome biogenesis factors from nascent 60S ribosomal subunits. Cell *138*, 911-922.

van Heel, M., Harauz, G., Orlova, E.V., Schmidt, R., and Schatz, M. (1996). A new generation of the IMAGIC image processing system. J Struct Biol *116*, 17-24.

Figure 1

Click here to download high resolution image

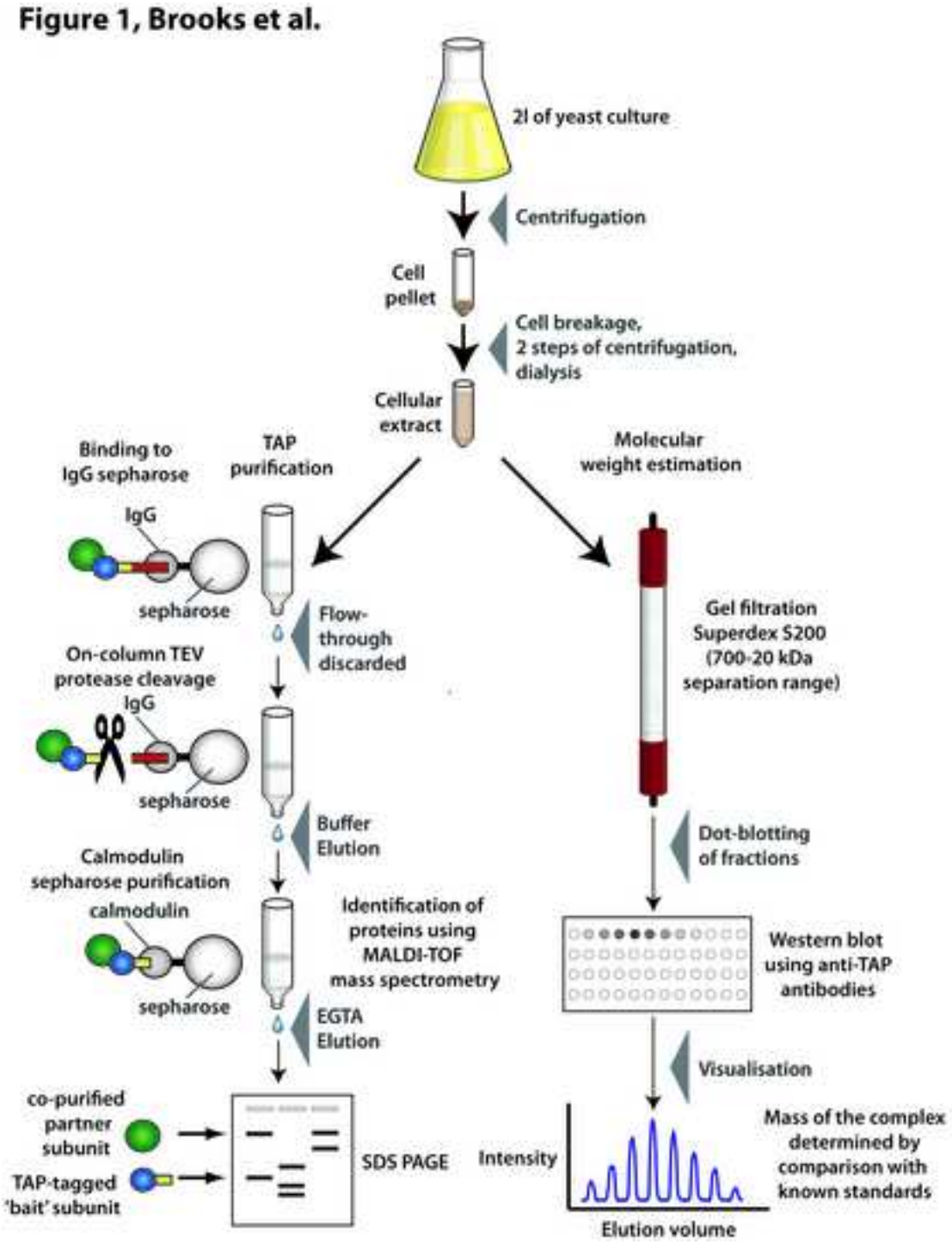

Figure 2

Click here to download high resolution image

Figure 2, Brooks et al.

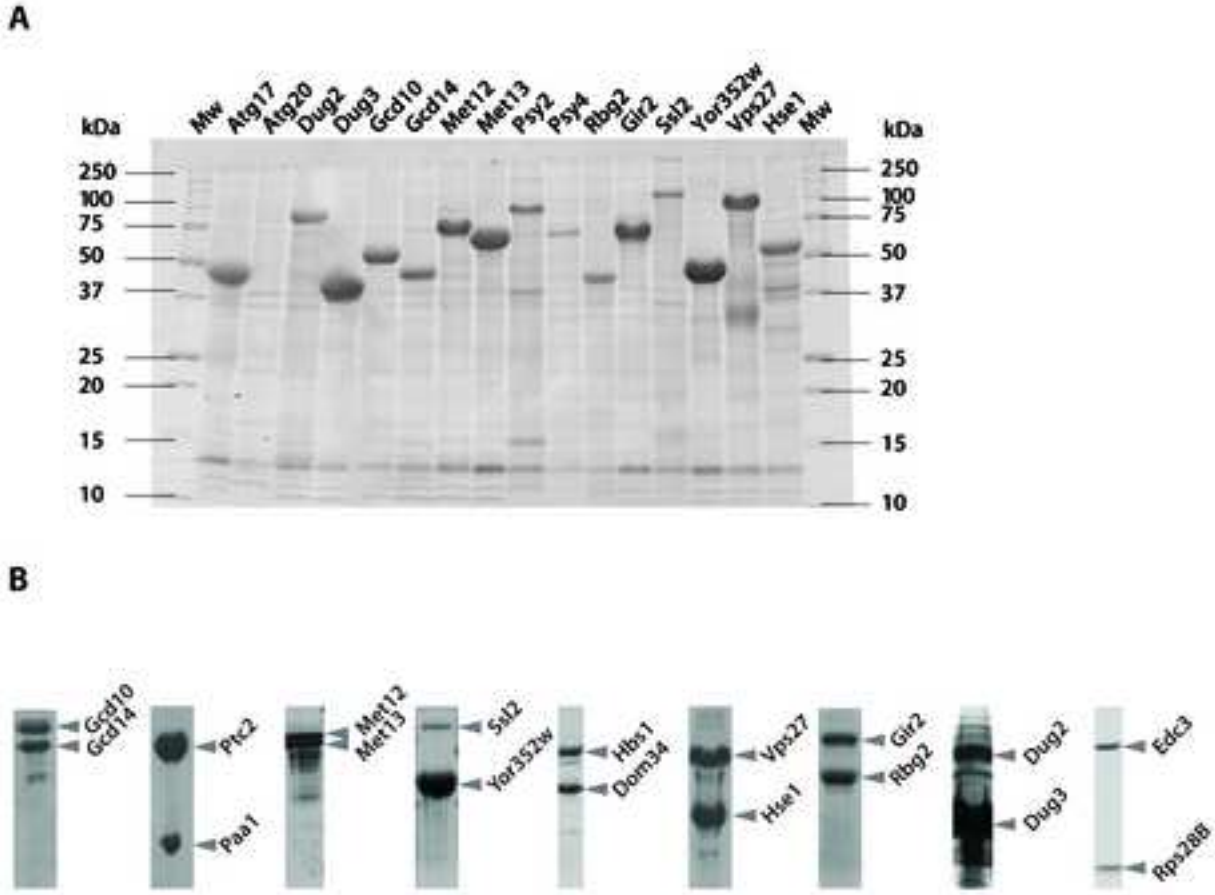

Figure 3

Click here to download high resolution image

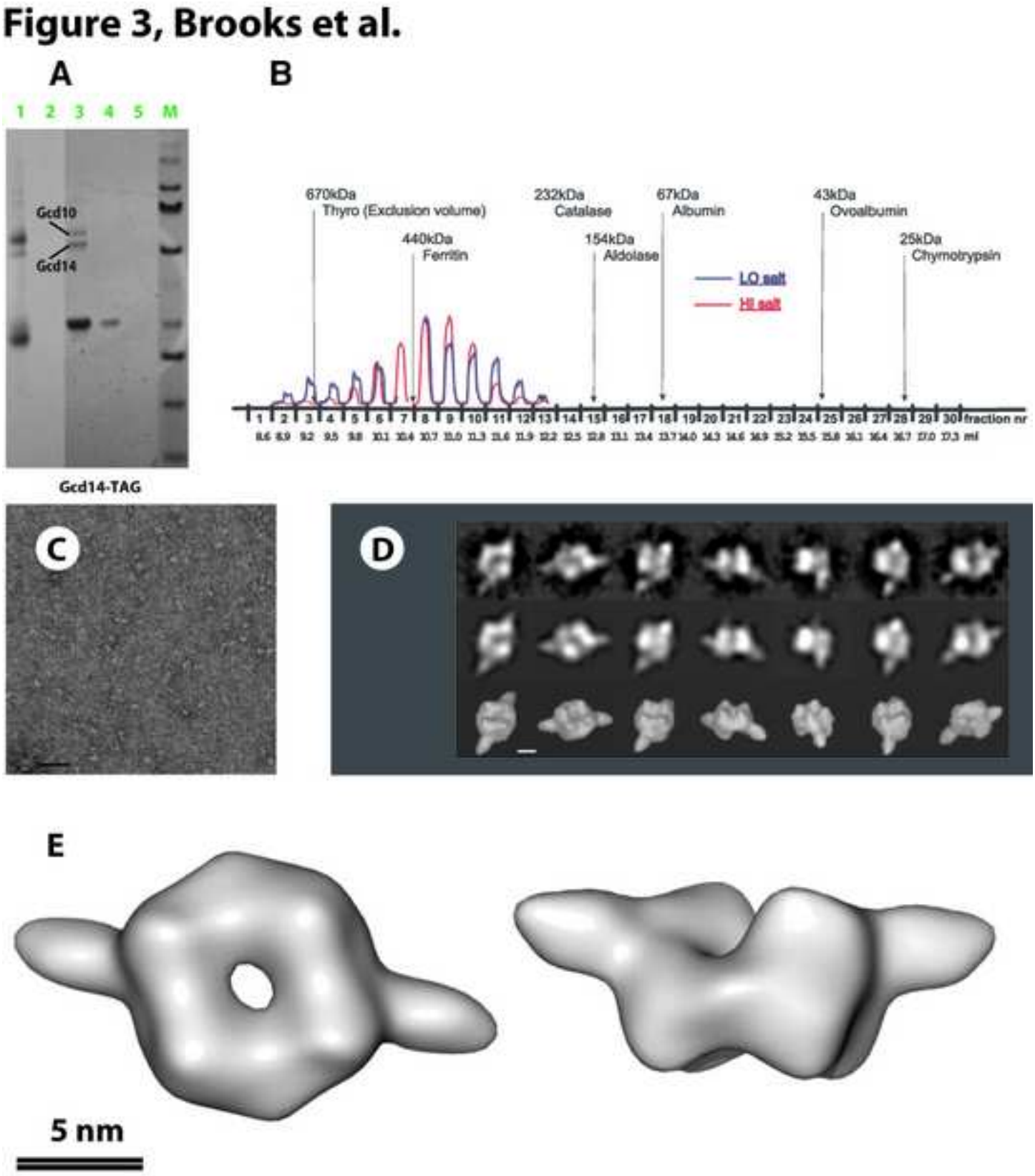

Inventory of Supplemental Information

Name	Summary	Related element in main text
Table S1	Bioinformatics triage: Non-redundant and manually curated set of 39 distinct yeast complexes of known 3D structure.	Table 1
Table S2	Bioinformatics triage: Final weights and effects of each parameter on the final selection.	Table 1
Table S3	Bioinformatics triage: Results of bioinformatics triage of Gavin et al complexes.	Table 1
Table S4	Manual triage: Lists of stoichiometric complexes identified by visual inspection of gels.	Table 1
Figure S1	Experimental validation of complexes.	Figure 1
Figure S2	Expression & Solubility Trials	Figure 2
Figure S3	Paa1-Ptc2 Complex Reconstitution	Figure 2
Figure S4	Vps27-Hse1 Complex Reconstitution	Figure 2
Figure S5	Gcd10-Gcd14 Complex Reconstitution	Figure 2
Figure S6	Ste11-Ste50 Complex Reconstitution	Figure 2
Figure S7	Effects of expression using synthetic genes using codon optimization relative to naturally occurring genes	Figure 2
Supp. Experimental Procedures		Experimental Procedures
Supp. References		References specific to the Supplementary Material

Supplemental Data

Supplemental Tables

Supplemental Table 1: *Non-redundant and manually curated set of 39 distinct yeast complexes of known 3D structure.*

Dotted horizontal lines indicate the thresholds corresponding to the complexes in the top 10 and top 50, after weight optimizations. Columns two and three show the accession codes of the corresponding PDB entries and the ORF IDs of the different yeast proteins in the given complex, respectively. Column 4 contains the feasibility score of the complex when ranking the 39 yeast complexes of known 3D structure together with the 491 complexes defined by Gavin *et al.*, 2006, and column 5 depicts the corresponding rank.

Complex description	PDB entries	Yeast ORF IDs	Feasibility score	Rank
Crystal structure of the yeast kinetochore Spc24/Spc25 globular domain	2FTX 2FV4	YER018C YMR117C	92	2
Elongation factor complex EEF1A:EEF1BA	1f60 1G7C 1IJE 1IJF	YAL003W YBR118W	91.74	3
RabGDP-dissociation inhibitor in complex with prenylated YPT1 GTPase	1UKV 2BCG	YER136W YFL038C	91.55	5
Mediator MED7/MED21 subcomplex	1YKE	YDR308C YOL135C	91.48	6
Sec23/24 heterodimer	1M2V	YIL109C YPR181C	90.76	7
20S proteasome	1G0U 1G65 1JD2 1RYP 2F16 2FNY	YBL041W YER012W YER094C YFR050C YGL011C YGR135W YGR253C YJL001W YML092C YMR314W YOL038W YOR157C YOR362C YPR103W	89.07	12
Ribonucleotide reductase Y2Y4 heterodimer	1JK0	YGR180C YJL026W	87.22	16
Structure of a Vps23-C:Vps28-N subcomplex	2F6M	YCL008C YPL065W	84.49	25
Mitochondrial processing peptidase	1HR6 1HR7 1HR8 1HR9	YHR024C YLR163C	83.65	29
Carboxypeptidase Y inhibitor complexed with the cognate proteinase	1WPX	YLR178C YMR297W	83.2	31
AHA1/HSP90 complex	1USU 1USV	YDR214W YPL240C	82.23	33
Eukaryotic clamp loader (RFC) bound to the DNA sliding clamp (PCNA)	1SXJ	YBR087W YBR088C YJR068W YNL290W YOL094C YOR217W	81.28	36
Mms2/Ubc13 ubiquitin conjugating enzyme complex	1JAT	YDR092W YGL087C	81.13	37
MLC1P bound to IQ2 of MYO2P	1M45 1N2D	YGL106W YOR326W	81	38
Heterodimer between H48F-ySOD1 and yCCS	1JK9	YJR104C YMR038C	79.97	42
TFIIA/TBP/DNA complex	1NH2 1RM1 1YTF	YER148W YOR194C	79.35	46
A conjugating enzyme/ubiquitin thiolester complex	1FXT	YDR177W YLR167W	79.1	47
Translation initiation factor eIF4E in complex with m7GDP and eIF4GI	1RF8	YGR162W YOL139C	78.9	48
ESCRT-II endosomal trafficking complex	1U5T 1W7P	YLR417W YPL002C YJR102C	78.89	49
Nucleosome core particle	1ID3	YBL002W YBR009C YBR010W YDR225W	78.46	50
SRP receptor beta-subunit in complex with the SRX domain from the alpha-subunit	1NRJ	YDR292C YKL154W	78.12	52
Brf1/TBP/DNA ternary complex	1NGM	YER148W YGR246C	78.04	54
Sec23/Sar1 complex	1M2O	YPL218W YPR181C	77.34	61
Dsk2p UBA/ubiquitin complex	1WR1	YIL148W YMR276W	76.77	63
A peptide:N-glycanase-Rad23 complex	1X3W 1X3Z	YEL037C YPL096W	74.66	75

RNA polymerase II	1NT9 1I50 1I6H 1NIK 1R5U 1R9S 1R9T 1SFO 1TWA 1TWC 1TWF 1TWG 1TWH 1I3Q 1K83 1WCM 1Y1W 1Y77 2B63	YBR154C YDL140C YDR404C YGL070C YHR143W-A YIL021W YJL140W YOL005C YOR151C YOR210W YOR224C YPR187W	72.96	88
Exportin CSE1P in complex with its cargo (KAP60P) and RanGTP	1WA5	YGL238W YLR293C YNL189W	72.24	91
RNA polymerase II/TFIIS complex	1PQV 1Y1V 1Y1Y	YBR154C YDL140C YDR404C YGL043W YGL070C YHR143WA YIL021W YJL140W YOL005C YOR151C YOR210W YOR224C YPR187W	71.21	94
MATa2/MCM1/DNA ternary transcription complex	1MNM	YCL067C YMR043W	69.62	103
CUE/ubiquitin complex	1OTR	YIL148W YKL090W	68.32	119
Cytochrome BC1 complex	1EZV 1KB9 1P84	Q0105 YBL045C YDR529C YEL024W YFR033C YGR183C YJL166W YOR065W YPR191W	64.61	151
MATa1/MATalpha2-3A heterodimer bound to DNA	1AKH 1LE8 1YRN	YCL067C YCR097W	64.19	157
Cytochrome BC1 complex with bound substrate cytochrome C	1KYO	Q0105 YBL045C YDR529C YEL024W YFR033C YGR183C YJL166W YJR048W YOR065W YPR191W	64.17	158
Electron transfer Complex between cytochrome C and cytochrome C peroxidase	1S6V 1U74 2B0Z 2B10 2B11 2B12 2BCN	YJR048W YKR066C	63.26	167
C-terminal ULP1 protease domain in complex with SMT3	1EUV	YDR510W YPL020C	56.86	218
YPD1/SLN1 response regulator domain complex	1OXB	YDL235C YIL147C	56.71	222
Solution Structure of Ede1 UBA-ubiquitin complex	2G3Q	YLR167W YBL047C	56.35	225
Lif1p/Lig4p complex	1Z56	YGL090W YOR005C	53.77	244
Orc1p/Sir1p complex	1ZBX 1ZHI	YKR101W YML065W	52.94	253

Supplemental Table 2: *Final weights and effects of each parameter on the final selection. *;*

Partial scoring function	Default weight	Contribution to the final score
Average socio-affinity index	1	30.3 %
Maximum individual protein weight	0.3	9.1 %
Total sequence length	0.1	3.0 %
Average number of problematic residues	0*	0 %
Co-localization ratio	0	0 %
Yeast two-hybrid ratio	1	30.3 %
Complete orthologs ratio	0.1	3.0 %
Average orthologs ratio	0.1	3.0 %
Self-consistency	0.4	12.1 %

Proteins with trans-membrane helices were excluded from the analysis.

Supplemental Table 3: *Results of bioinformatics triage of Gavin et al complexes.*

Complex ID	Subunits	Rank	Score
1	Ste11, Ste50	1	100
2	Atg17, Atg29, Atg11	27	85.96
3	Vps27, Hse1	1	100
4	Psy2, Psy4, Pph3	4	99.17
5	Nup82, Nup159, Nsp1	4	99.17
6	Ede1, Syp1	22	87.14
7	Dop1, Mon2	25	86.43

Supplemental Table 4A: *List of stoichiometric dimeric complexes identified by visual inspection of gels.*

No.	Subunits		Gels (with hyperlinks)
1.	Gsy1	Gsy2	SC-PG-245-SC2550(1)-5
2.	Trr1	Trr2	SC-PG-286-SC3097(1)-9 SC-PG-291-SC3169(1)-4
3.	Gdc14	Gdc10	SC-PG-260-SC2835(1)-4
4.	Bur2	Svg1	SC-PG-226-SC2187(1)-6 SC-PG-257-SC2387(1)-1
5.	Ptc2	Paa1	SC-PG-202-SC1898(1)-6 SC-PG-365-SC2732(3)-3
6.	Met12	Met13	SC-PG-264-SC3020(1)-9 SC-PG-277-SC2455(1)-4 SC-PG-264-SC3020(1)-9
7.	Snx41	Snx4	SC-PG-459-SC3504(4)-7 SC-PG-359-SC3504(2)-2 SC-PG-336-SC3724(1)-3 SC-PG-326-SC3504(1)-5
8.	Trm7	Ymr259c	SC-PG-447-SC3979(1)-9
9.	Fbf26	Ylr345w	SC-PG-283-SC2908(1)-1 SC-PG-389-SC0279(4)-4
10.	Ubp2	Rup1	SC-PG-366-SC4106(1)-2 SC-PG-422-SC4751(1)-5
11.	Skp1	Ymr258c	SC-PG-423-SC4814(1)-3
12.	Ydr221	Rot2	SC-PG-314-SC3454(1)-4
13.	Qcr1	Cor1	SC-PG-330-SC2395(3)-2
14.	Pep4	Rtn1	SC-PG-374-SC3088(2)-8 SC-PG-321-SC3088(1)-7
15.	Ram2	Cdc43	SC-PG-315-SC3602(1)-9
16.	Trm8	Trm82	SC-PG-313-SC3442(1)-5
17.	Ynl119w	Ybr281c	SC-PG-413-SC5018(1)-3
18.	Yml119w	Yll032c	SC-PG-413-SC5021(1)-5
19.	Ssl2	Yor352w	SC-PG-414-SC5032(1)-2
20.	Trm12	Trm112	SC-PG-182-SC1472(2)-5 SC-PG-112-SC1438(1)-3
21.	Pfk1	Pfk2	SC-PG-119-SC0365(1)-3
22.	Toa1	Toa2	SC-PG-122-SC1519(1)-8
23.	Sly1	Sec17 or Ykt6	SC-PG-126-SC0871(1)-6
24.	Isw1	Ioc3	SC-PG-206-SC1982(1)-9 SC-PG-133-SC0692(1)-4
25.	Apm3	Apl6	SC-PG-095-SC1063(1)-5 SC-PG-133-SC0725(1)-6
26.	Bmh1	Bmh2	SC-PG-137-SC1091(1)-3
27.	Wbp1	Swp1	SC-PG-188-SC1788(1)-7 SC-PG-148-SC0897(1)-6
28.	Sbf2	Sec23	SC-PG-295-SC2585(1)-9
29.	Sec24	Sec23	SC-PG-186-SC1621(1)-5 SC-PG-155-SC1144(1)-5
30.	Rat1	Rai1	SC-PG-164-SC1486(1)-4
31.	Spt16	Pob3	SC-PG-062-SC1012(1)-6 SC-PG-171-SC1329(1)-6
32.	Kgd2	Kgd1	SC-PG-094-SC0863(1)-1 SC-PG-025-SC0264(1)-5
33.	Rad53	Asf1	SC-PG-261-SC2359(2)-2 SC-PG-090-SC1168(1)-5
34.	Ser33	Ser3	SC-PG-030-SC0214(2)-2
35.	Uba3	Ula1	SC-PG-034-SC0411(1)-4 SC-PG-034-SC0410(2)-3
36.	Ceg1	Cet1	SC-PG-250-SC2369(1)-2
37.	Ybl046w	Psy2	SC-PG-106-SC1412(1)-2 SC-PG-043-SC0457(1)-7
38.	Bdf1	Bdf2	SC-PG-049-SC0788(1)-10
39.	Yku70	Yku80	SC-PG-231-SC2234(1)-8 SC-PG-055-SC1097(1)-3
40.	Spt6	Iws1	SC-PG-077-SC1036(2)-6
41.	Cap1	Cap2	SC-PG-078-SC1132(2)-1
42.	Rnr2	Rnr4	SC-PG-213-SC2035(1)-5 SC-PG-090-SC1153(1)-3
43.	Srp101	Srp102	SC-PG-131-SC0199(2)-4
44.	Gyl1	Gyp5	SC-PG-175-SC1593(1)-5 SC-PG-235-SC2246(1)-7
45.	Tfa1	Tfa2	SC-PG-305-SC3228(1)-7
46.	Nkp1	Nkp2	SC-PG-301-SC1937(1)-5
47.	Dcs1	Dcs2	SC-PG-278-SC2903(1)-9
48.	Nma1	Nma2	SC-PG-274-SC2907(1)-7
49.	Nrd1	Nab3	SC-PG-249-SC2362(1)-6 SC-PG-232-SC2290(1)-6
50.	Rvs161	Rvs167	SC-PG-248-SC1857(1)-1 SC-PG-341-SC3099(1)-8
51.	Clc1	Chc1	SC-PG-211-SC2033(1)-6 SC-PG-062-SC1011(1)-5
52.	Itc1	Isw2	SC-PG-123-SC1540(1)-3 SC-PG-210-SC2001(1)-1
53.	Pan2	Pan3	SC-PG-058-SC0987(1)-8

Supplemental Table 4B: *List of stoichiometric trimeric complexes identified by visual inspection of gels.*

No.	Subunits			Gels (with hyperlinks)
54.	Arc1	Mes1	Gus1	SC-PG-213-SC2048(1)-9 SC-PG-210-SC2011(1)-8
55.	Tef1/Tef2	Cam1	Efb1	SC-PG-249-SC2348(1)-2
56.	Lat1	Pda1	Pdb1	SC-PG-172-SC1752(1)-5 SC-PG-152-SC1390(1)-3
57.	Nup82	Nsp1	Nup159	SC-PG-151-SC1632(2)-5 SC-PG-121-SC1633(1)-6
58.	Hat1	Hat2	Hif1	SC-PG-033-SC0392(1)-1
59.	Tps1	Tps1	Tps3 or Tsl1	SC-PG-031-SC0596(1)-6 SC-PG-202-SC1899(1)-7 SC-PG-230-SC2218(1)-5 SC-PG-236-SC2254(1)-3

Supplemental Table 4C: *List of stoichiometric tetrameric complexes identified by visual inspection of gels.*

No.	Subunits				Gels (with hyperlinks)
60.	Cka1	Cka2	Ckb1	Ckb2	SC-PG-198-SC1820(1)-6 SC-PG-114-SC1485(1)-3
61.	Stp22	Ygr206w	Srn2	Vps28	SC-PG-310-SC3363(1)-8
62.	Spc25	Spc24	Nuf2	Tid3	SC-PG-369-SC4402(1)-6
63.	Rlr1	Hpr1	Thp1	Mft1	SC-PG-162-SC1405(1)-4
64.	Sec62	Sec66	Sec63	Sec72	SC-PG-306-SC2332(1)-6

Supplemental Figures

Supplemental Figure 1:

A

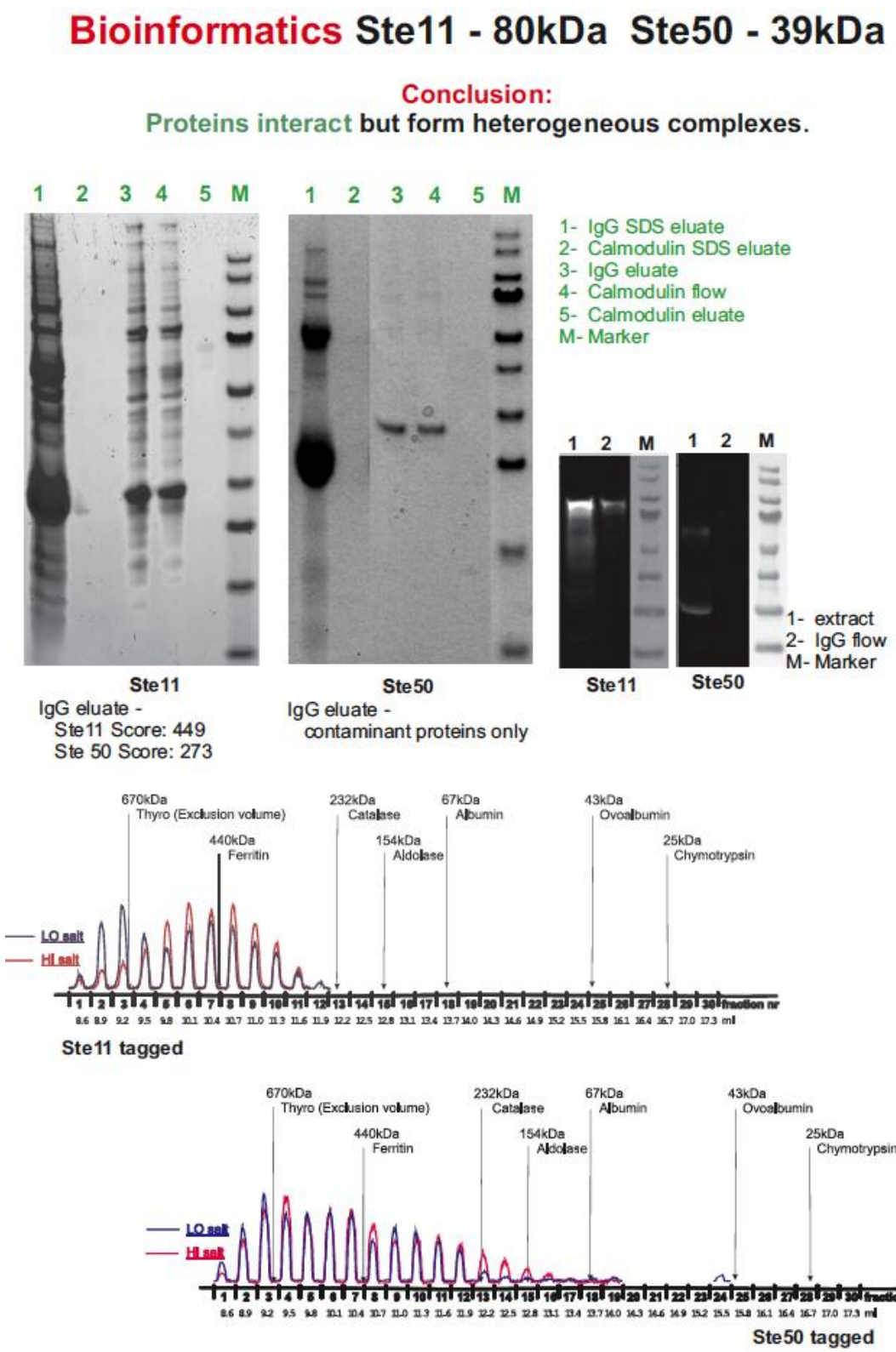

Supplemental Figure 1:

B

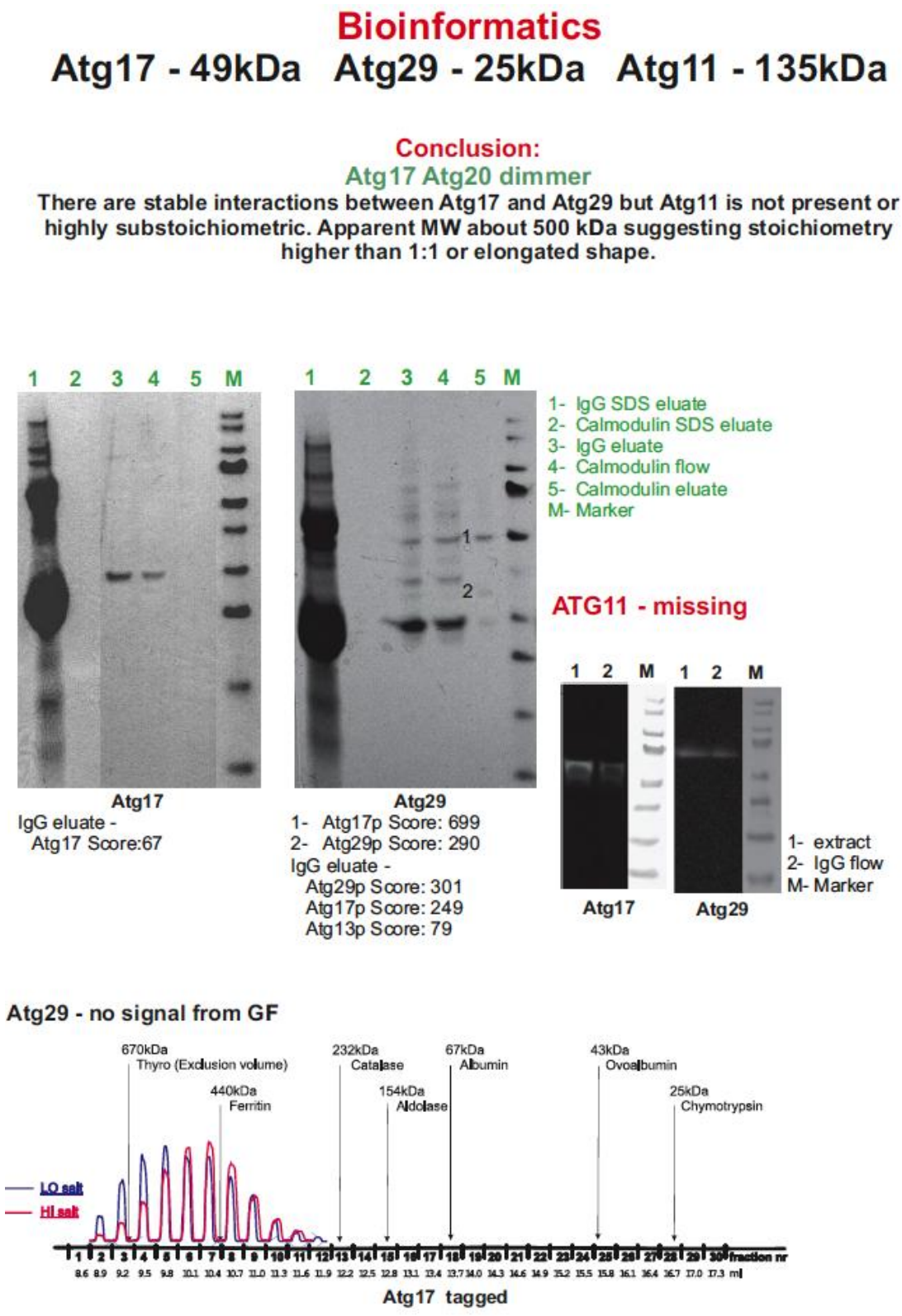

Supplemental Figure 1:

C

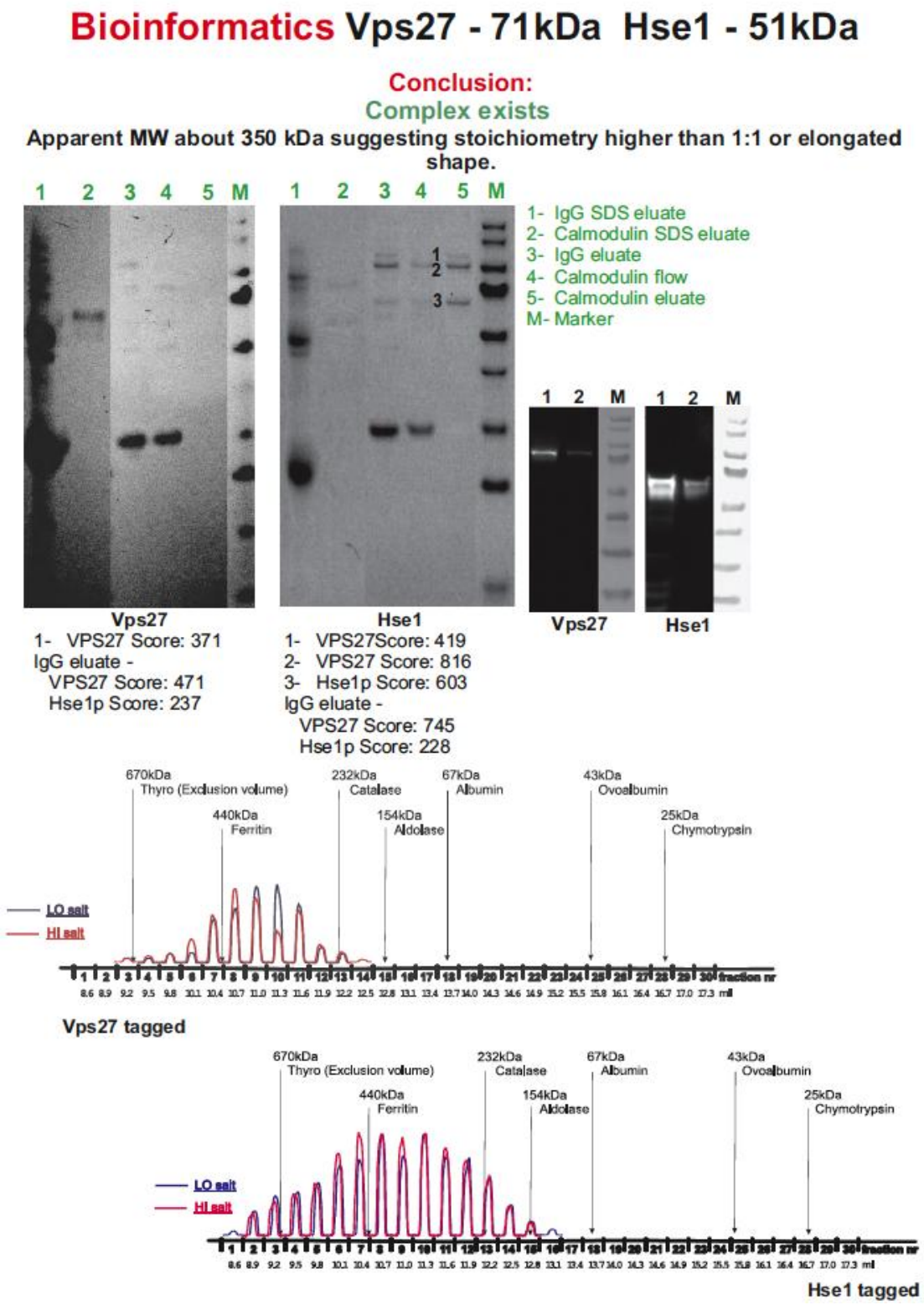

Supplemental Figure 1:

D

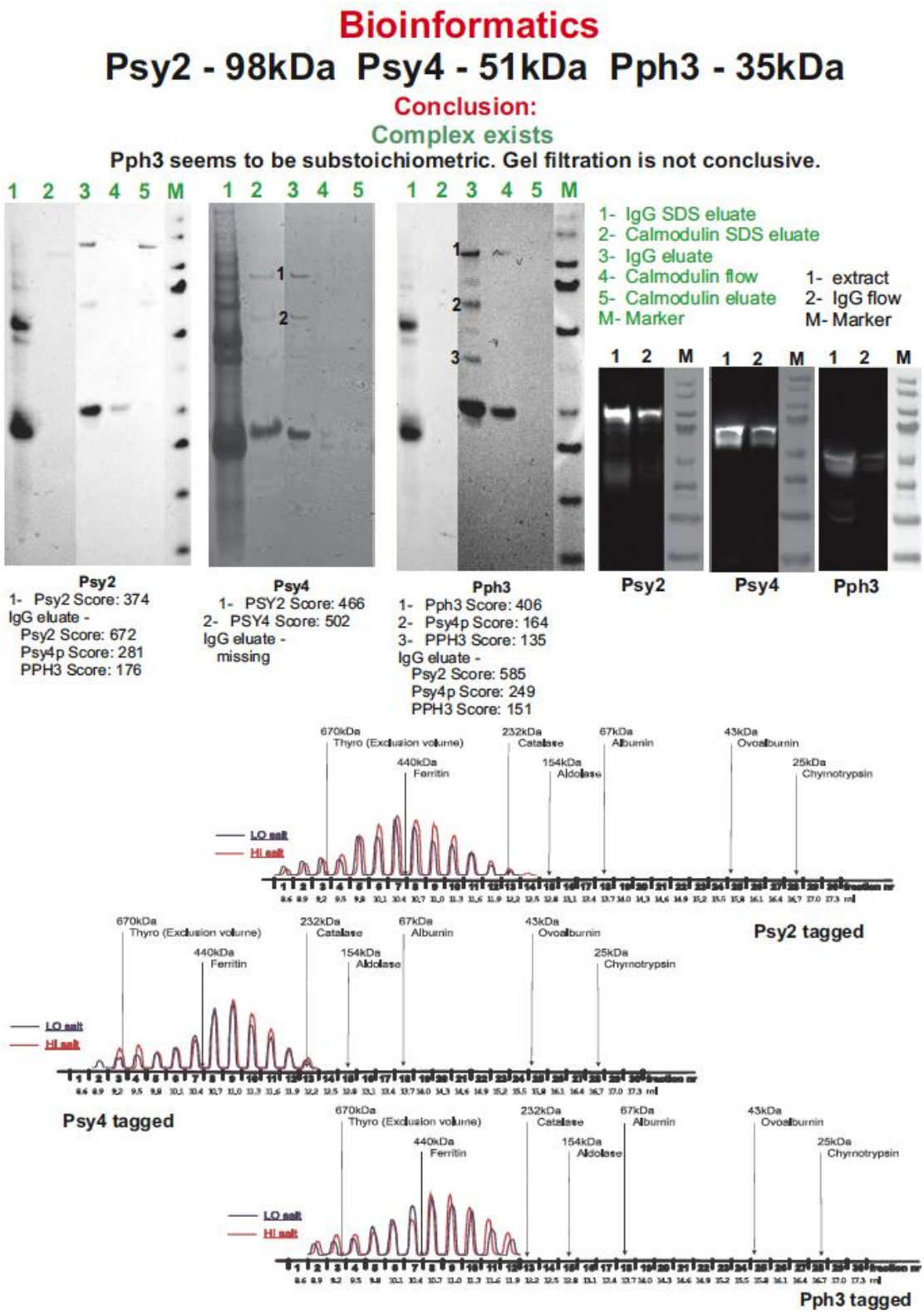

Supplemental Figure 1:

E

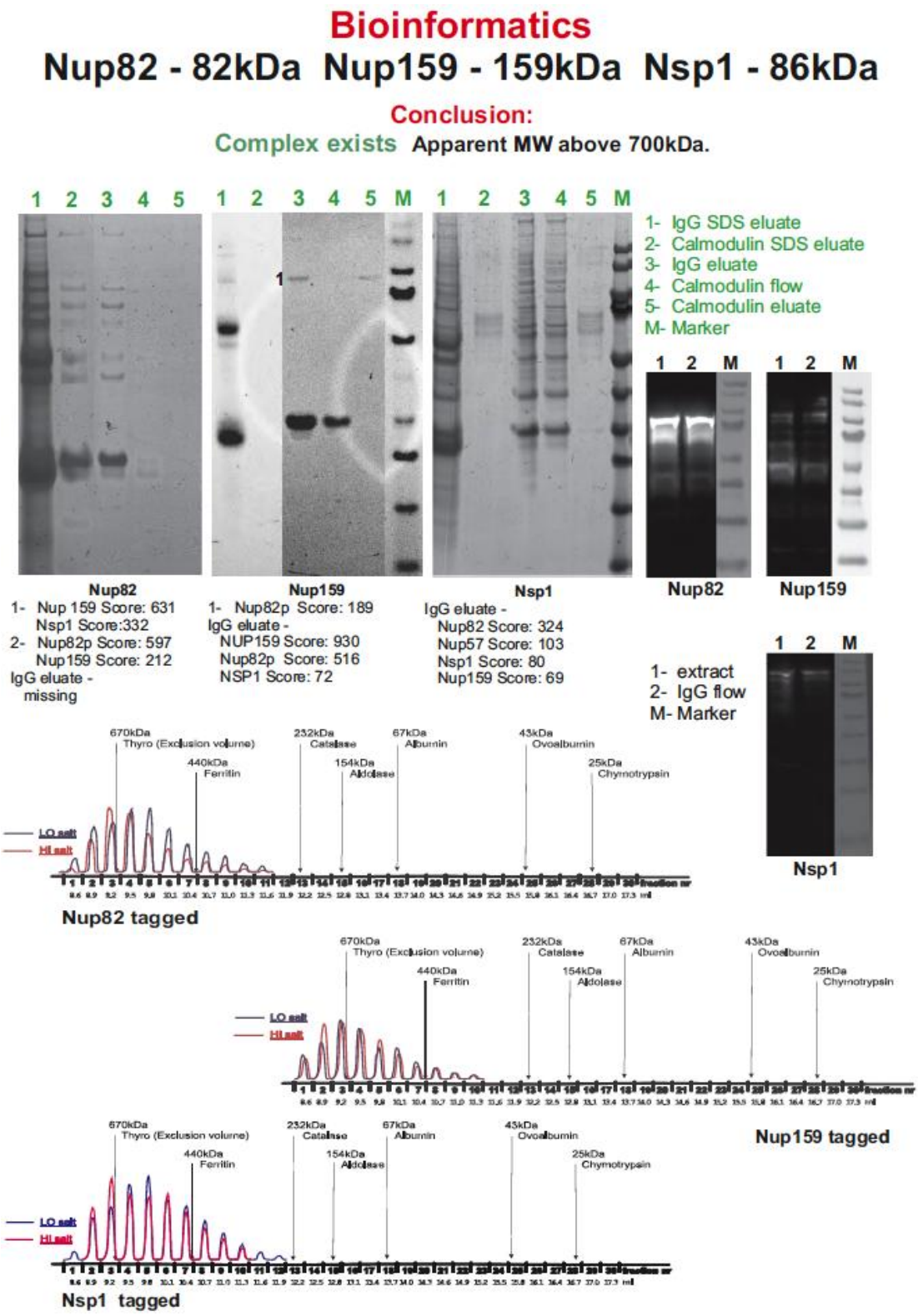

Supplemental Figure 1:

F

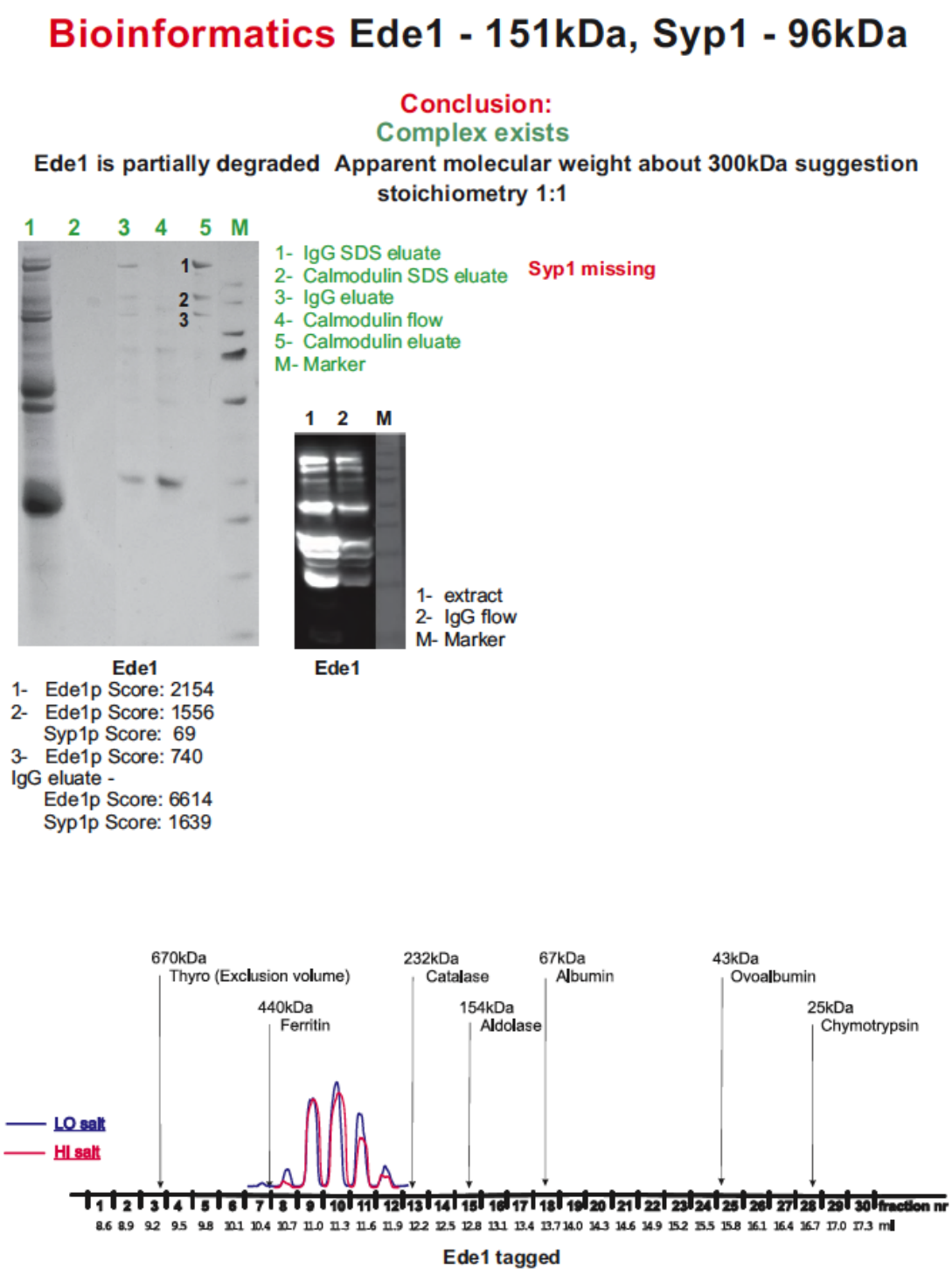

Supplemental Figure 1:

G

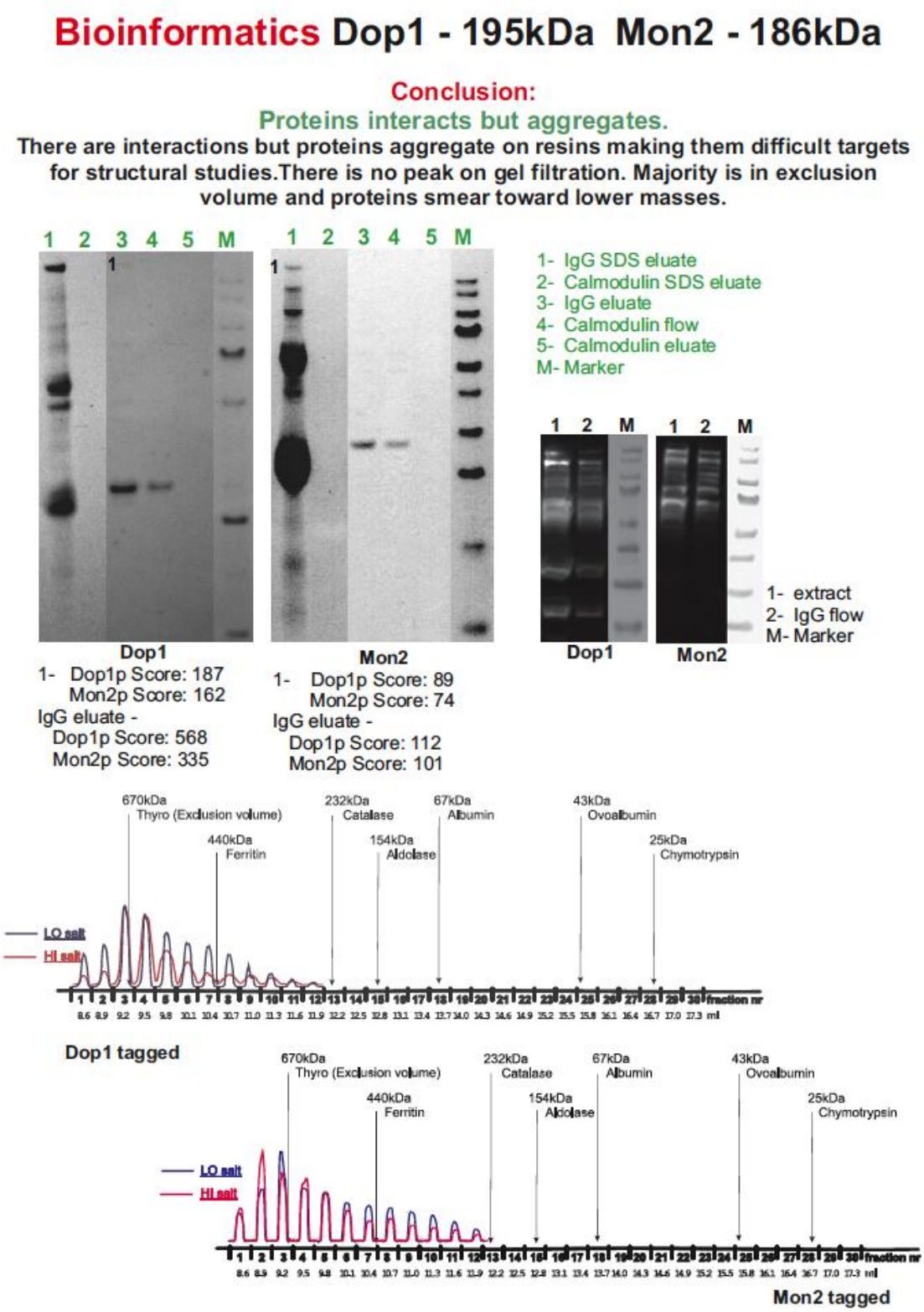

Supplemental Figure 1:

H

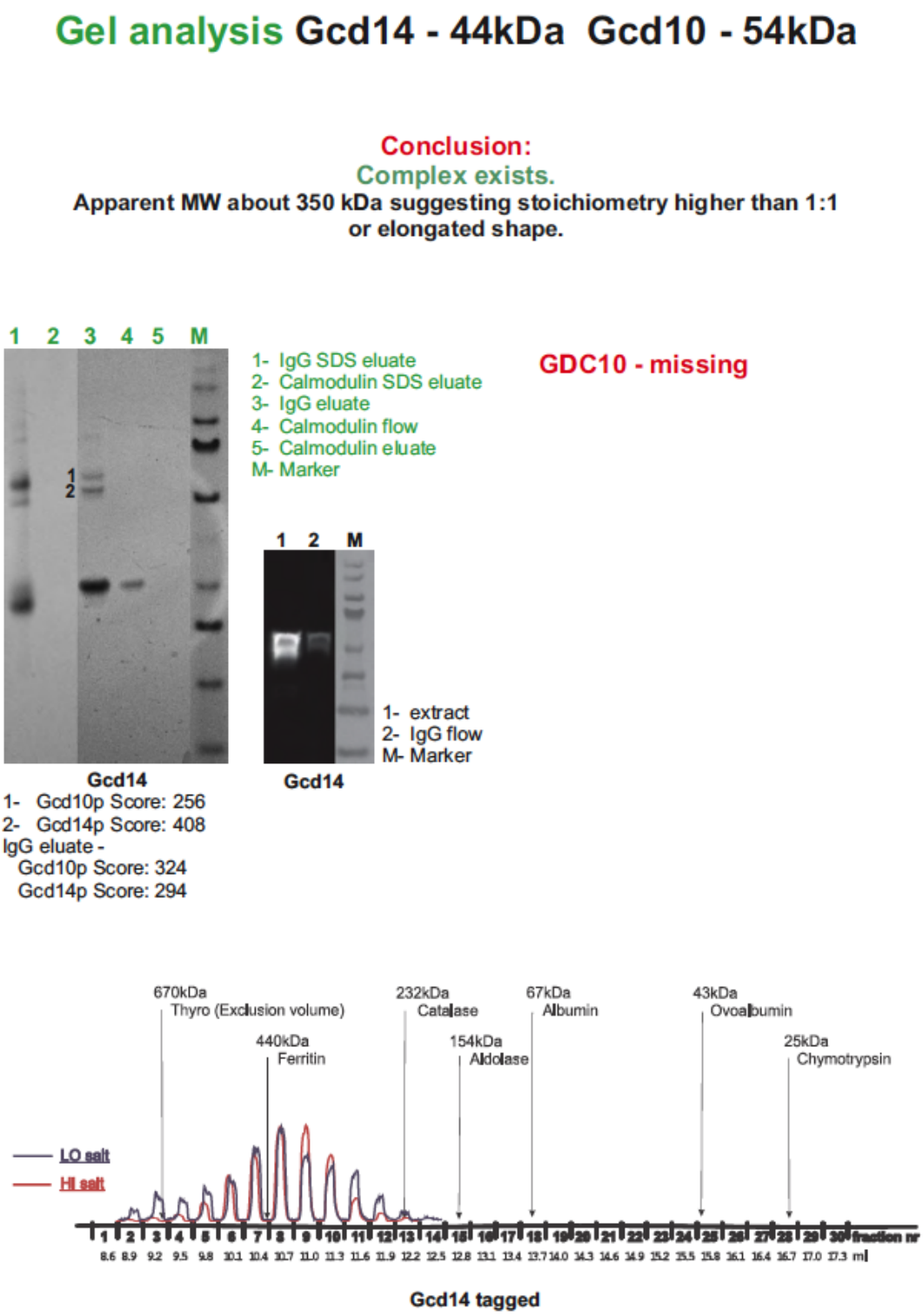

Supplemental Figure 1:

I

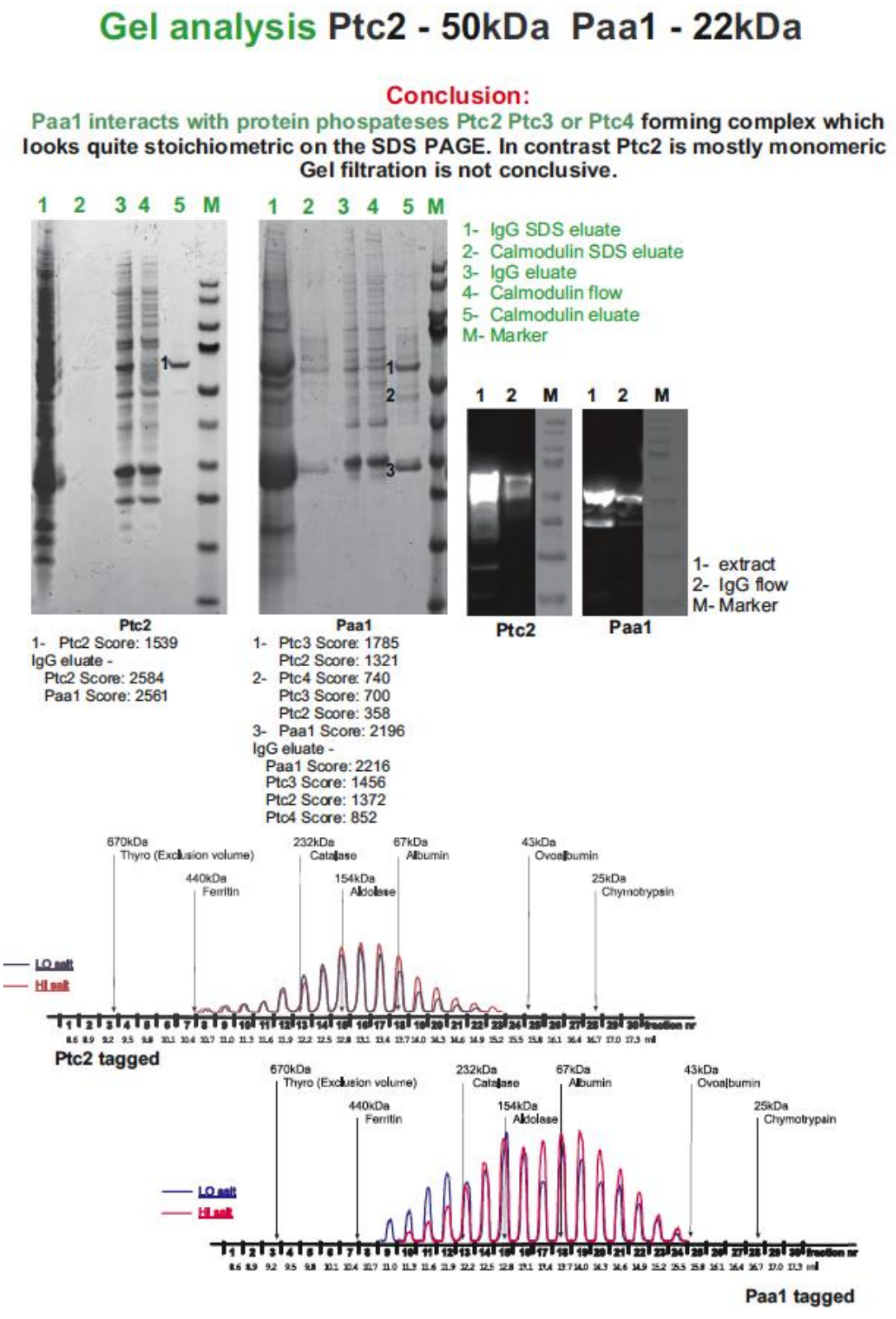

Supplemental Figure 1:

J

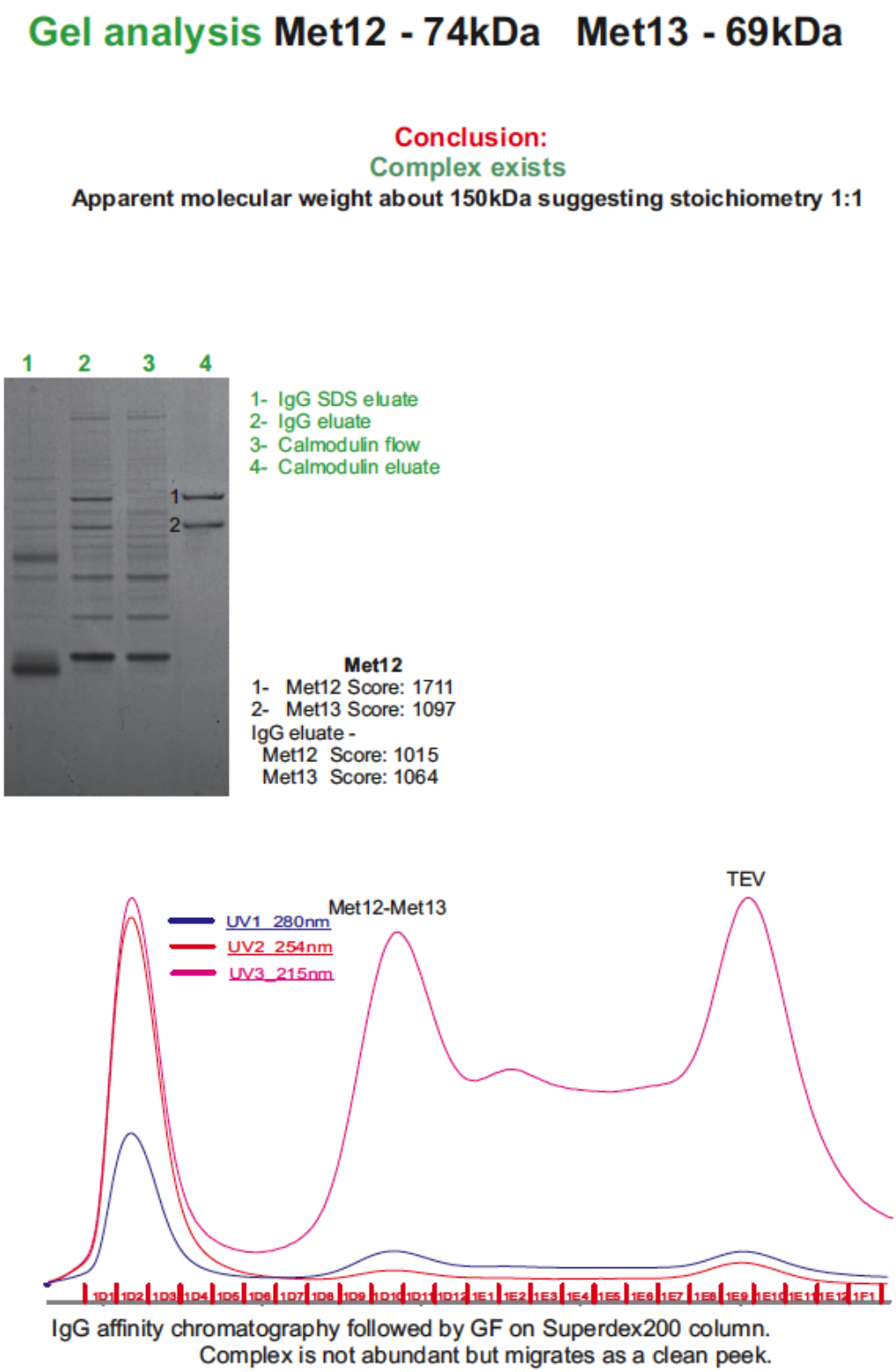

IgG affinity chromatography followed by GF on Superdex200 column.
Complex is not abundant but migrates as a clean peek.

Supplemental Figure 1:

K

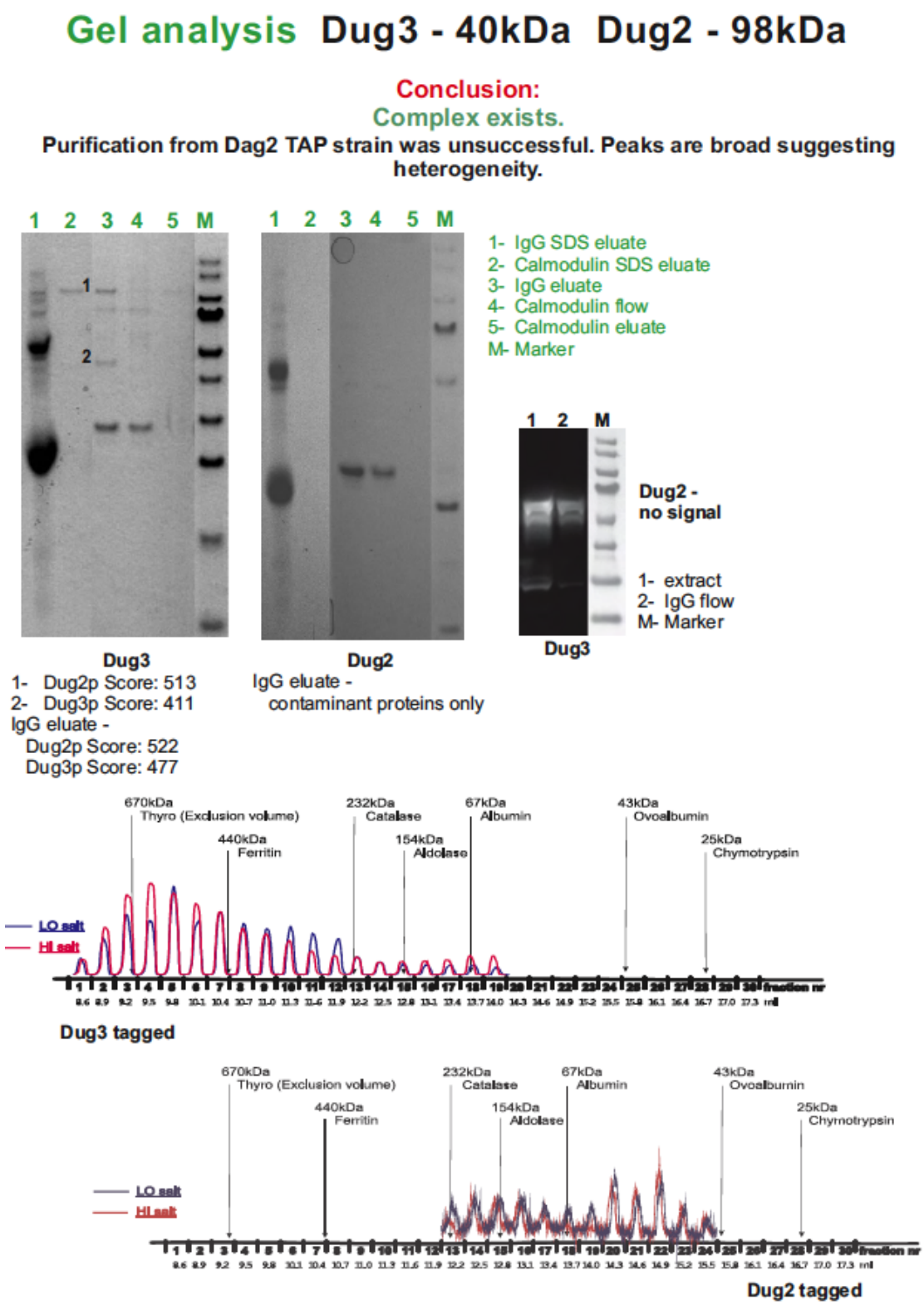

Supplemental Figure 1:

L

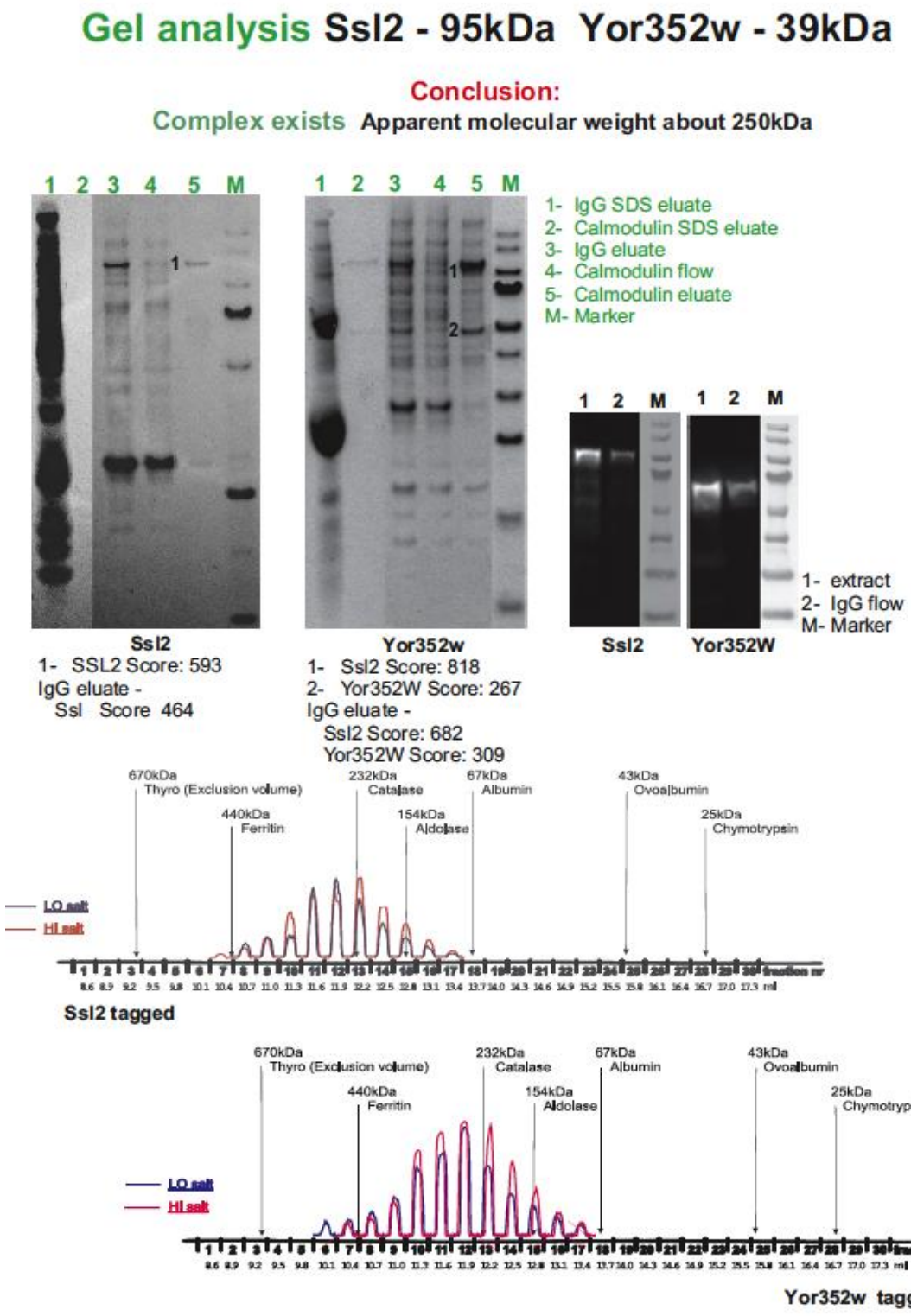

Supplemental Figure 1:

M

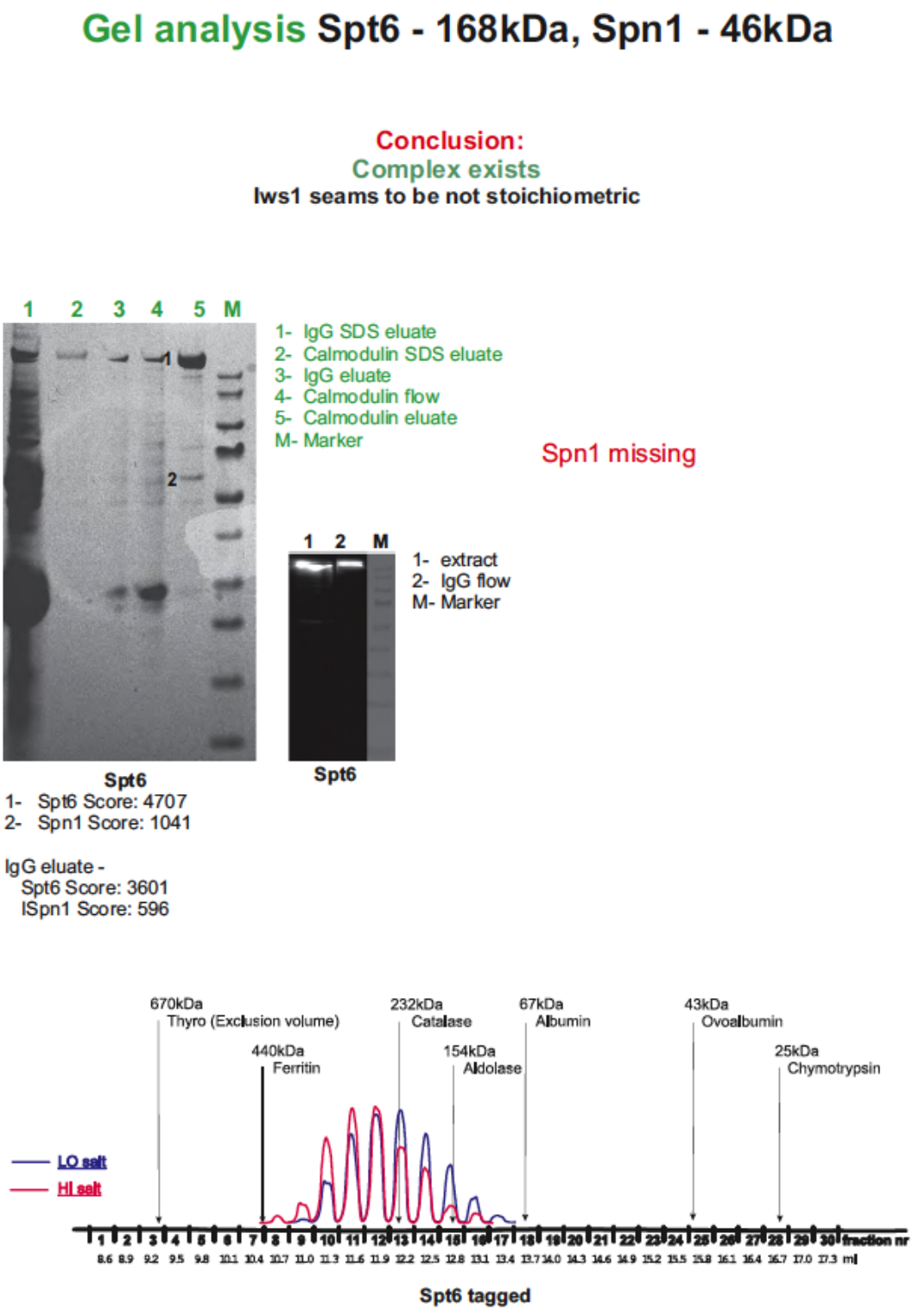

Supplemental Figure 1:

N

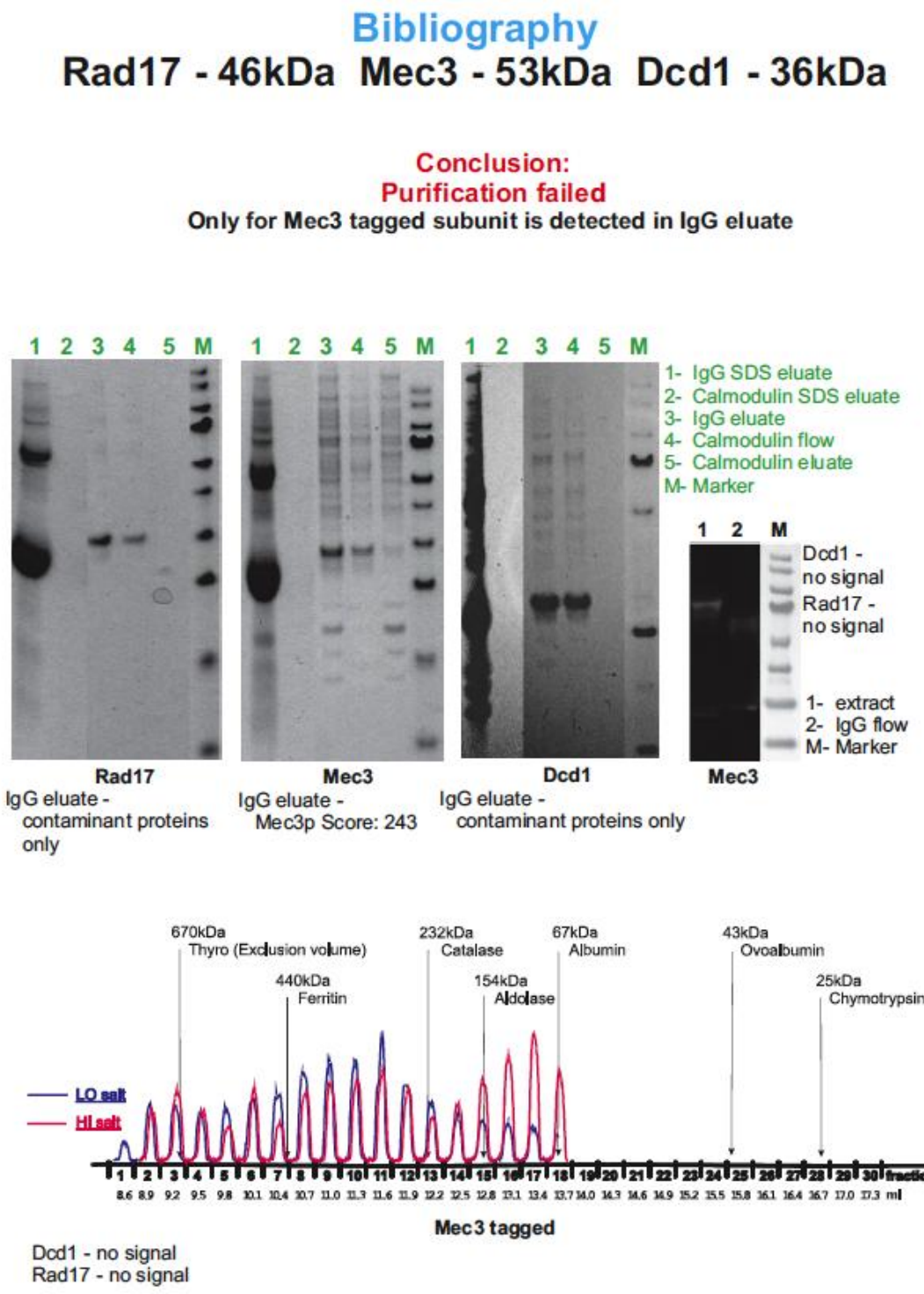

Supplemental Figure 1:

O

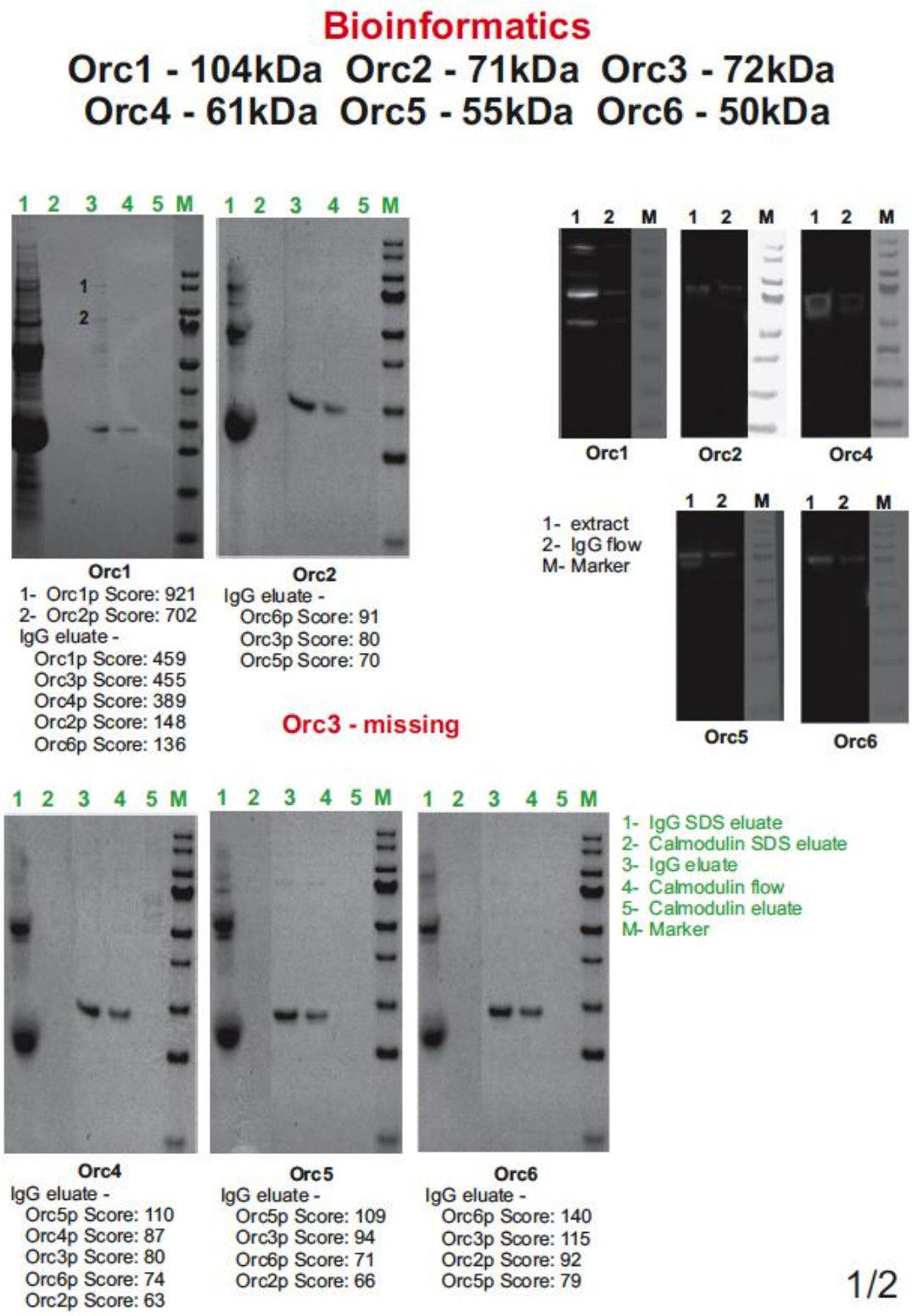

Supplemental Figure 1:

P

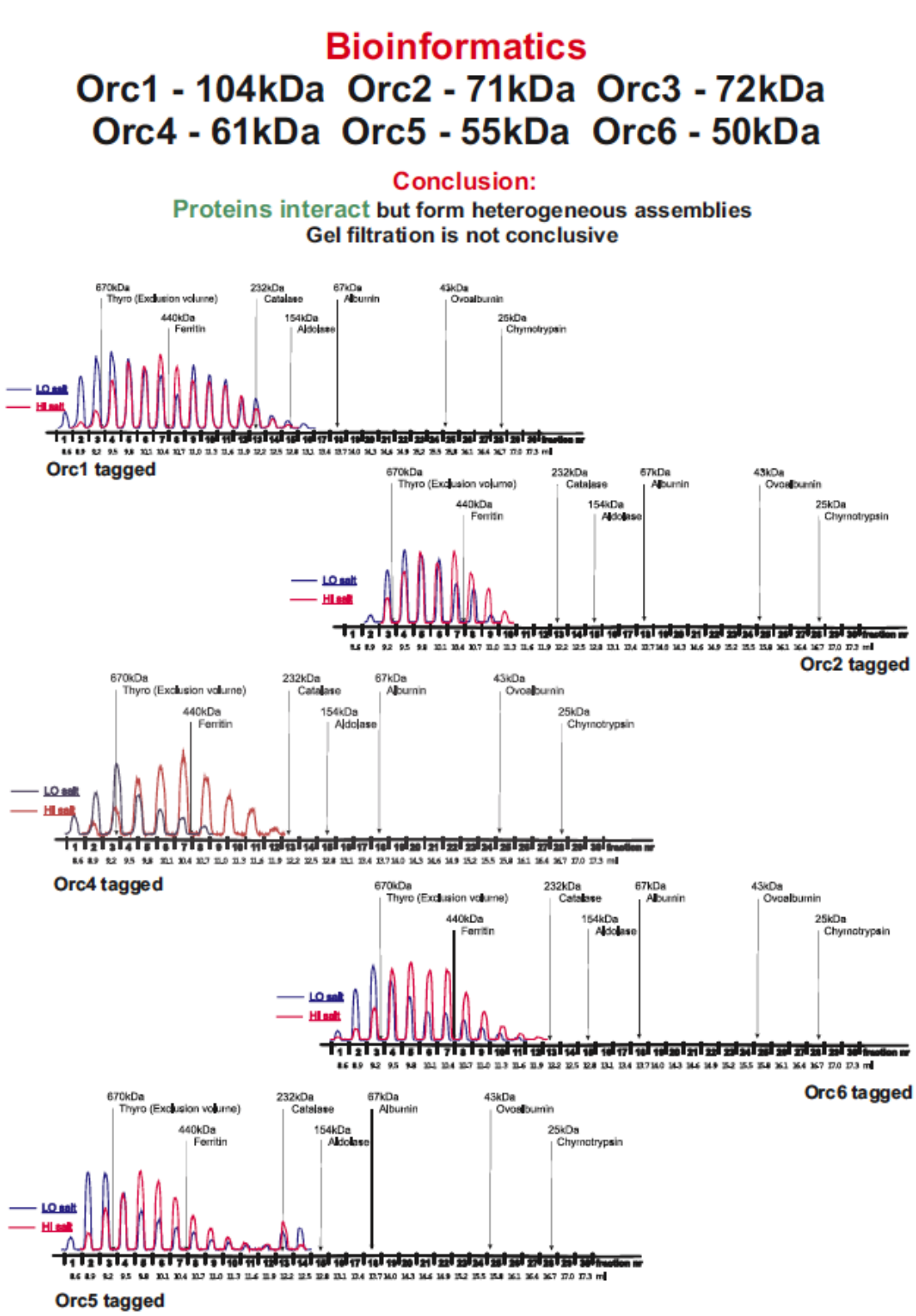

Supplemental Figure 1:

Q

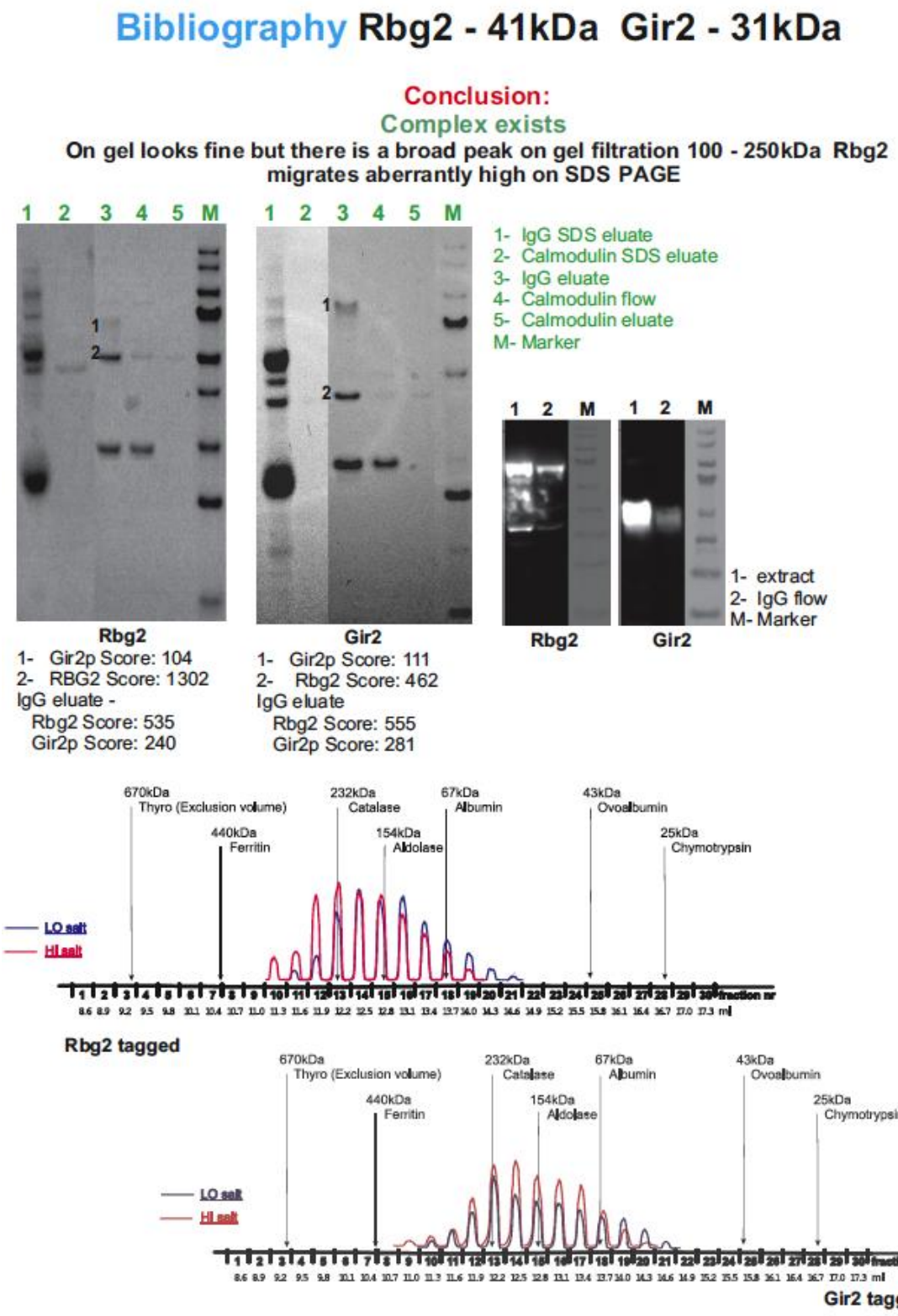

Supplemental Figure 1:

R

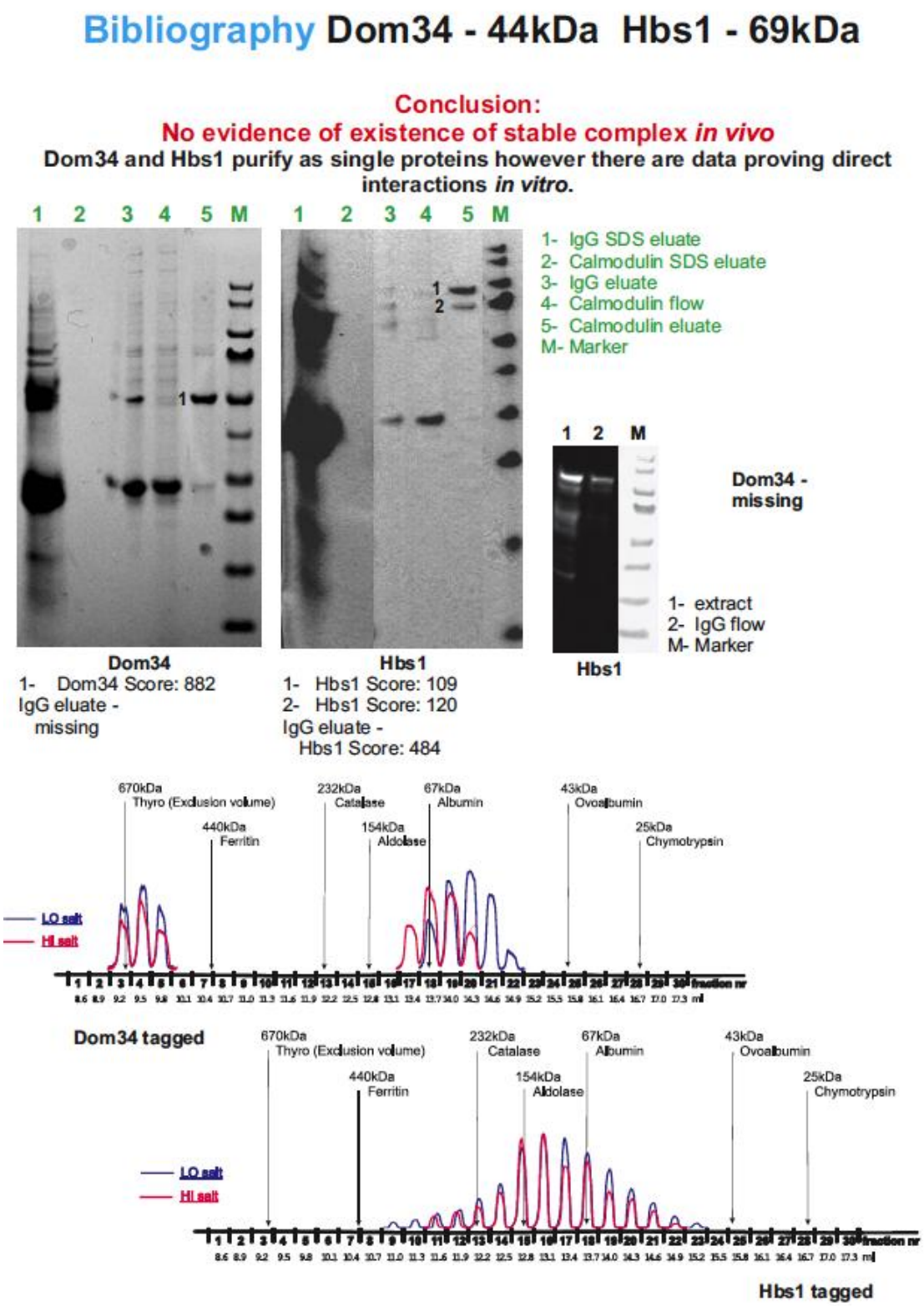

Supplemental Figure 1:

S

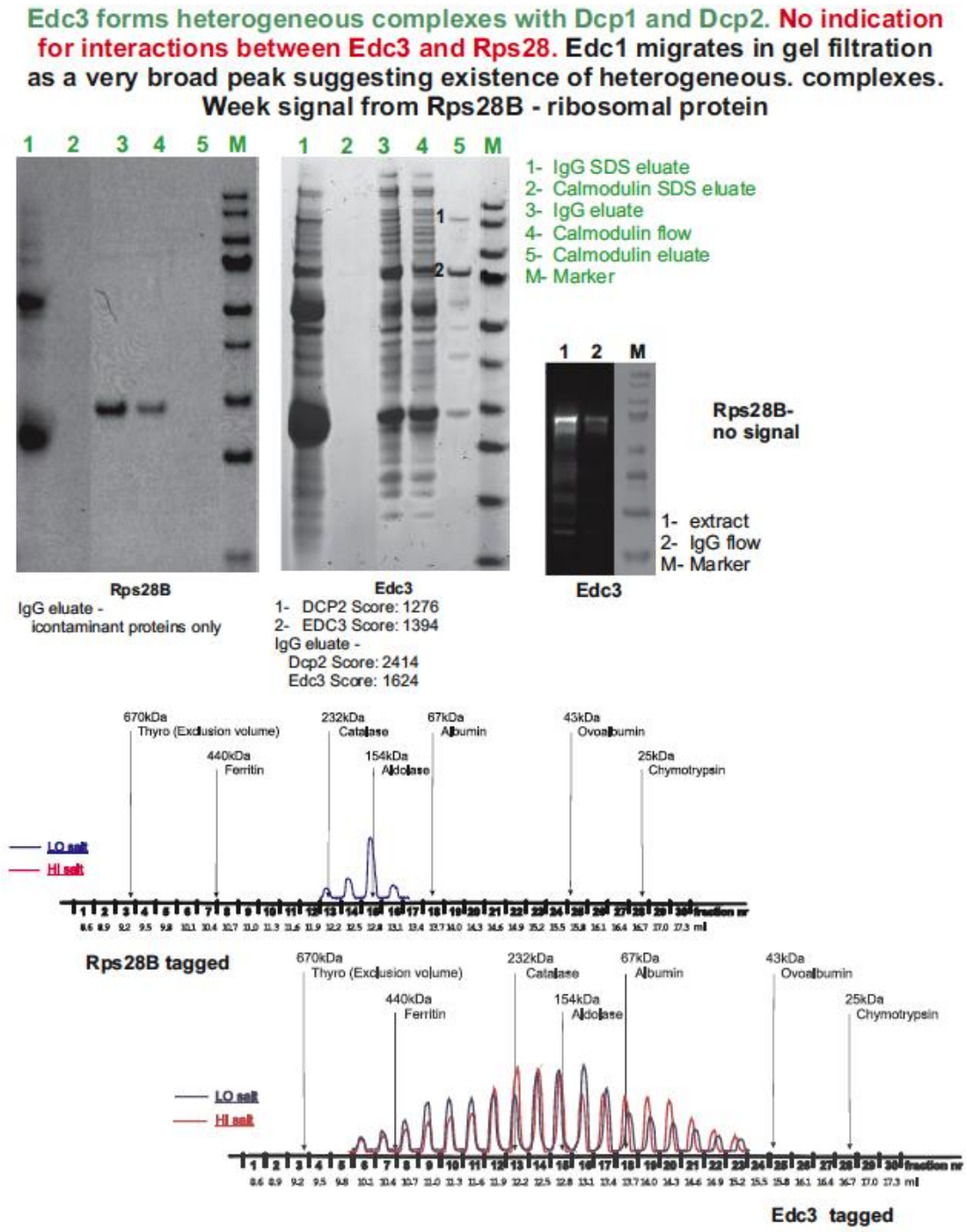

Supplemental Figure 1:

T

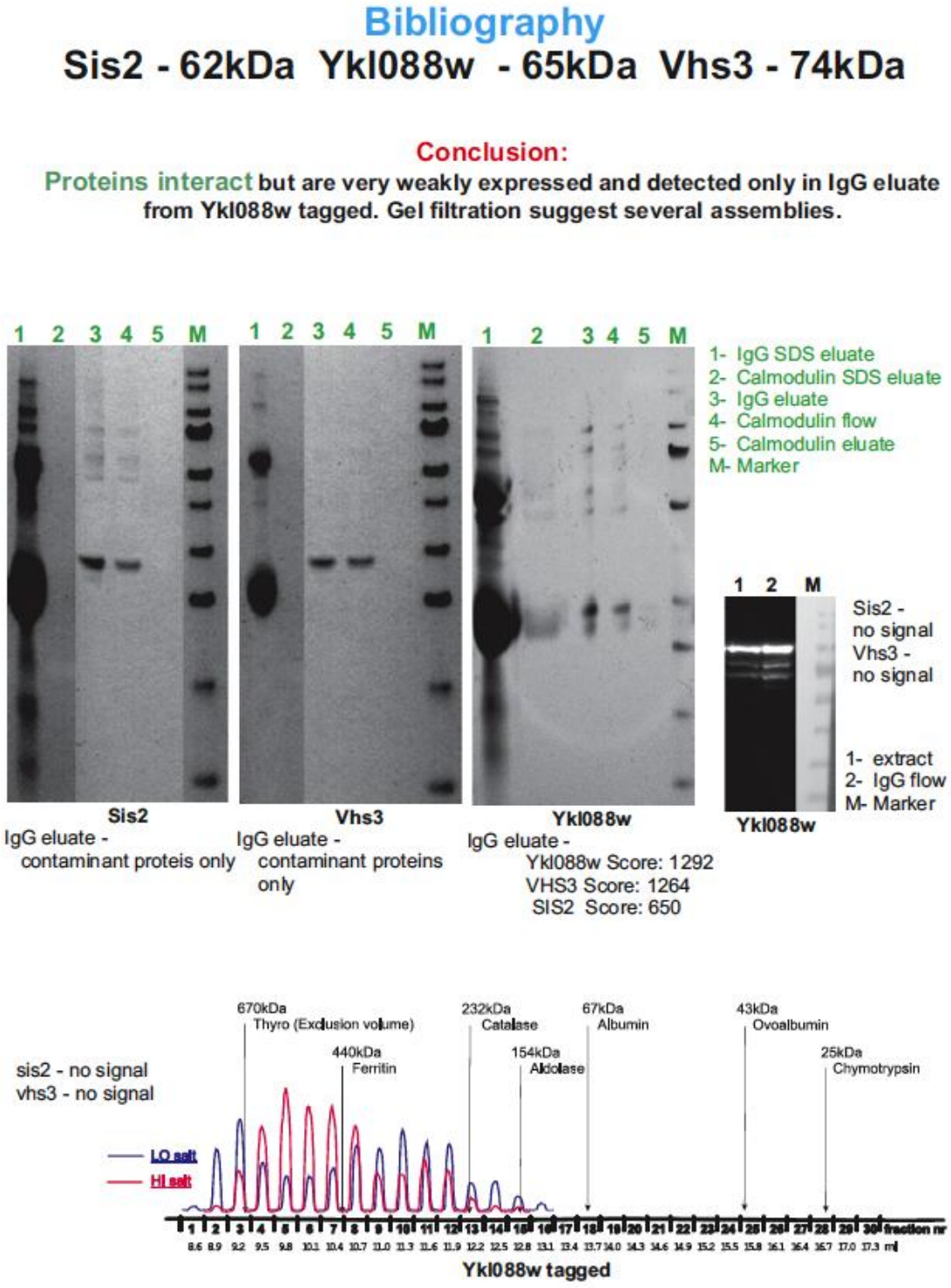

Supplemental Figure 1:

U

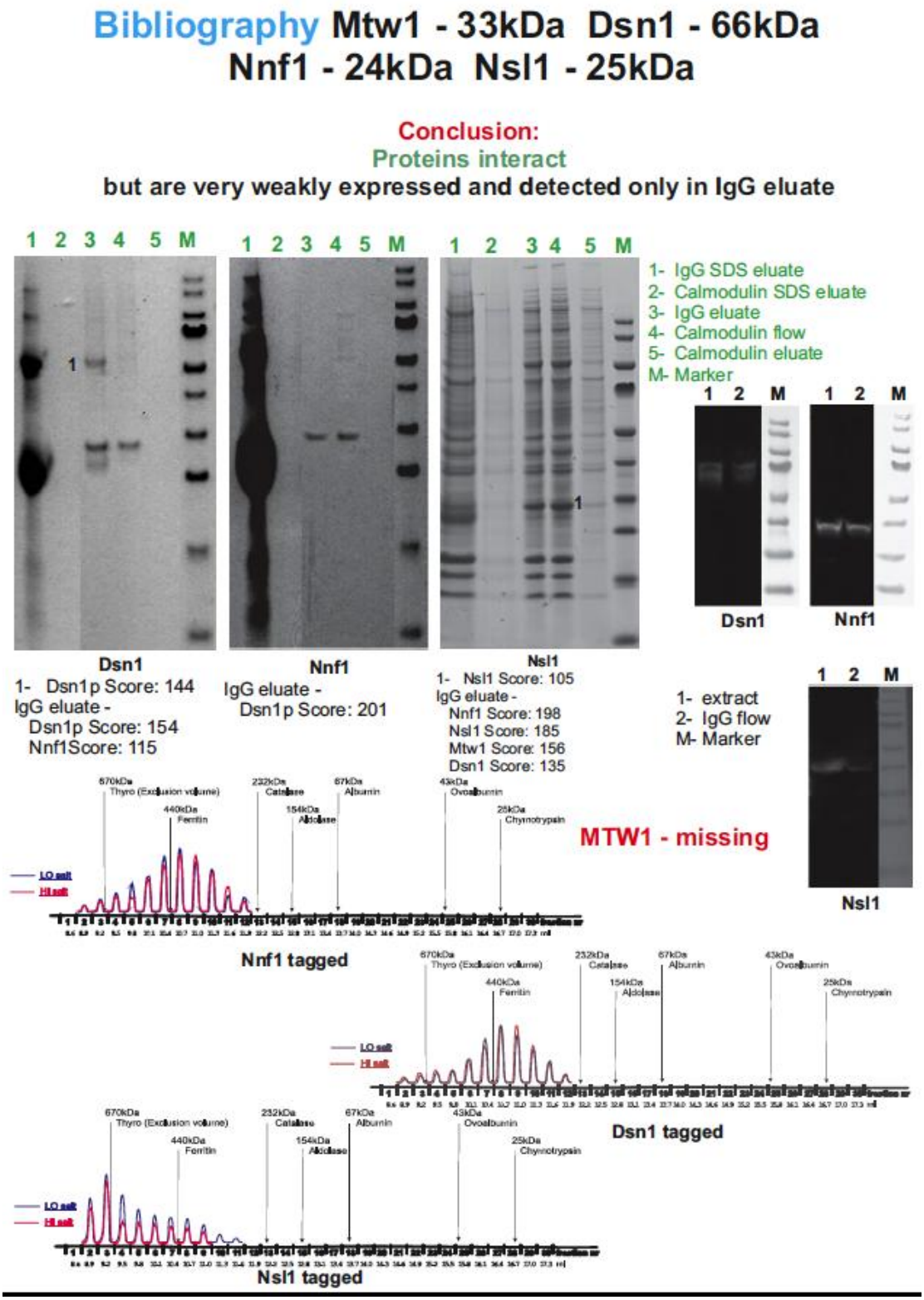

Supplemental Figure 2: Expression & Solubility Trials

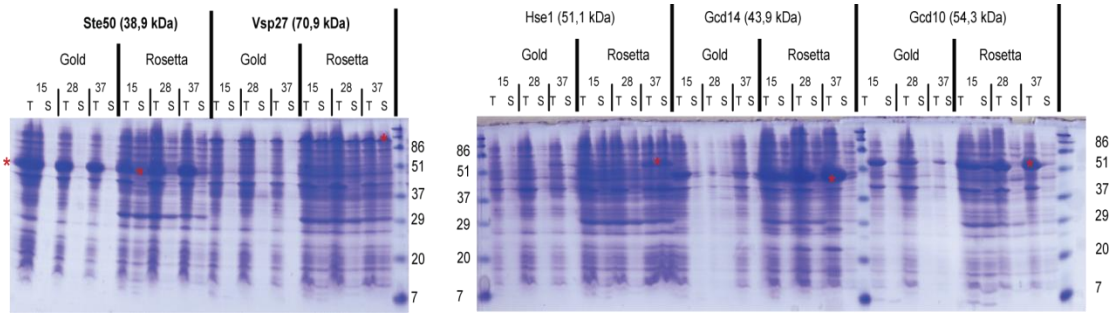

Supplemental Figure 3: Paa1-Ptc2 Purification & Complex Reconstitution Experiment

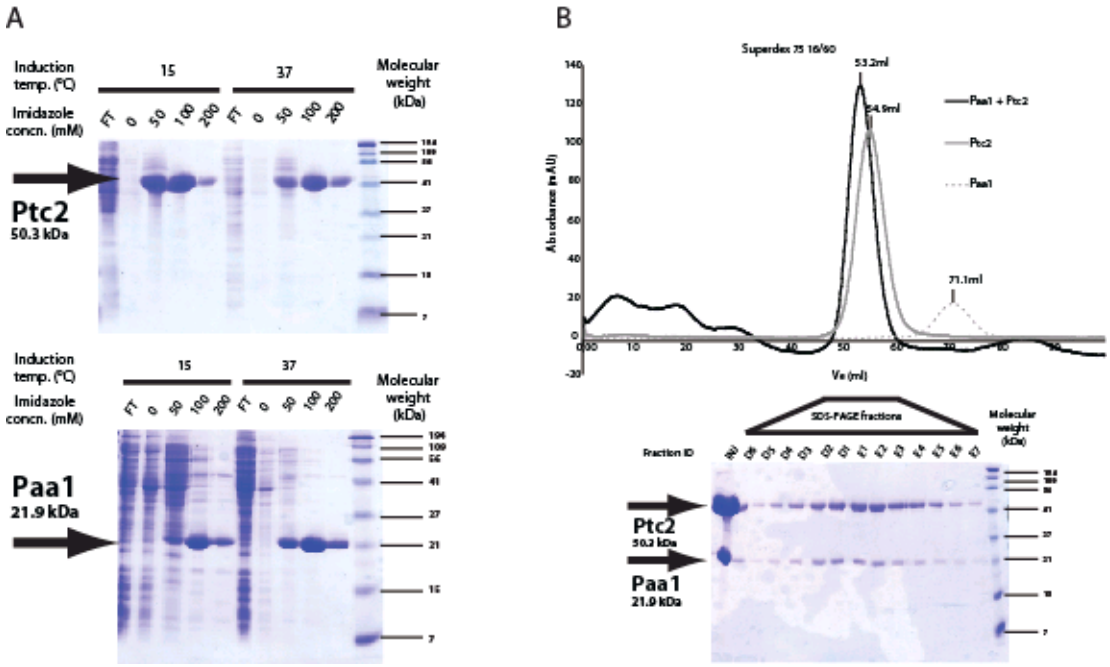

Supplemental Figure 4: Vps27-Hse1 Purification & Complex Reconstitution Experiment

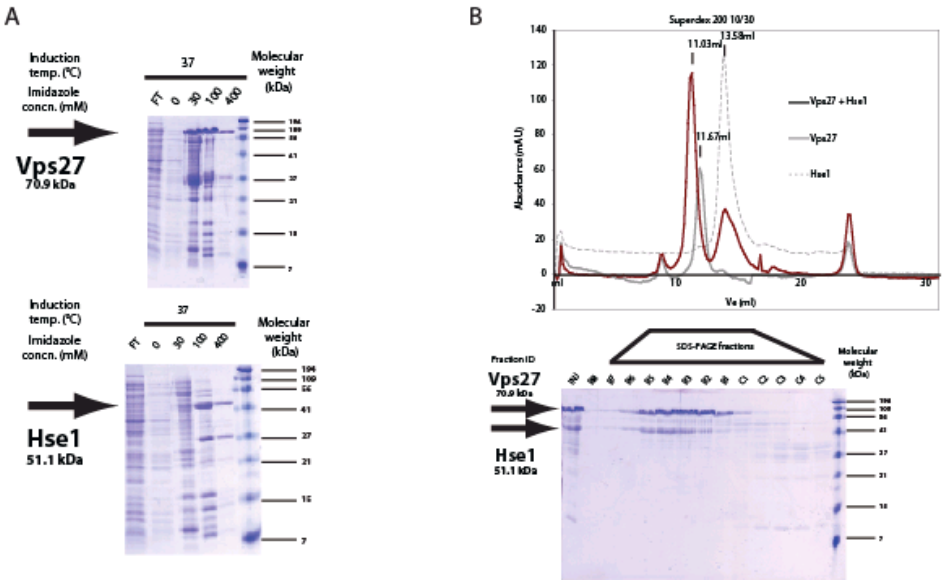

Supplemental Figure 5: Gcd10-Gcd14 Purification & Complex Reconstitution Experiment

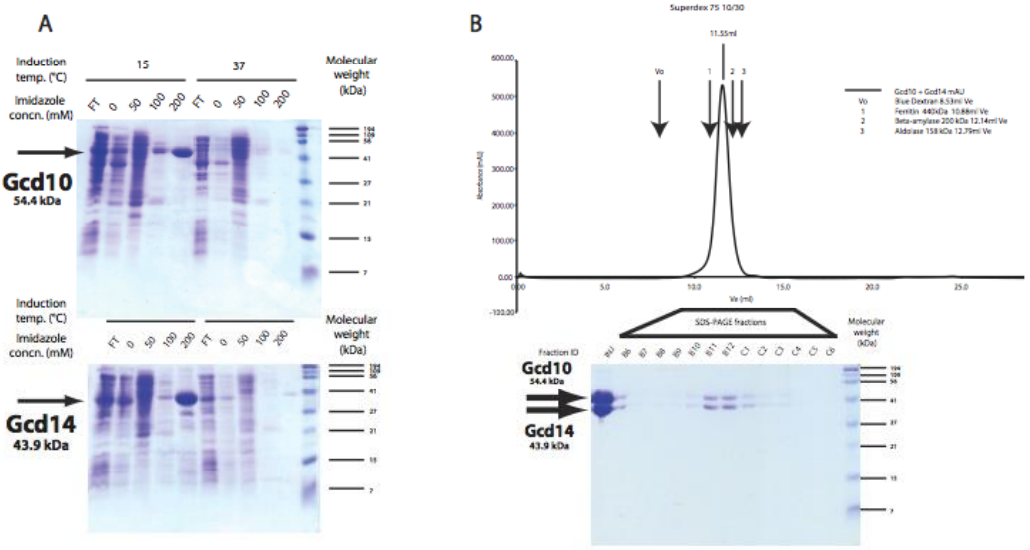

Supplemental Figure 6: Ste11-Ste50 Purification & Complex Reconstitution Experiment

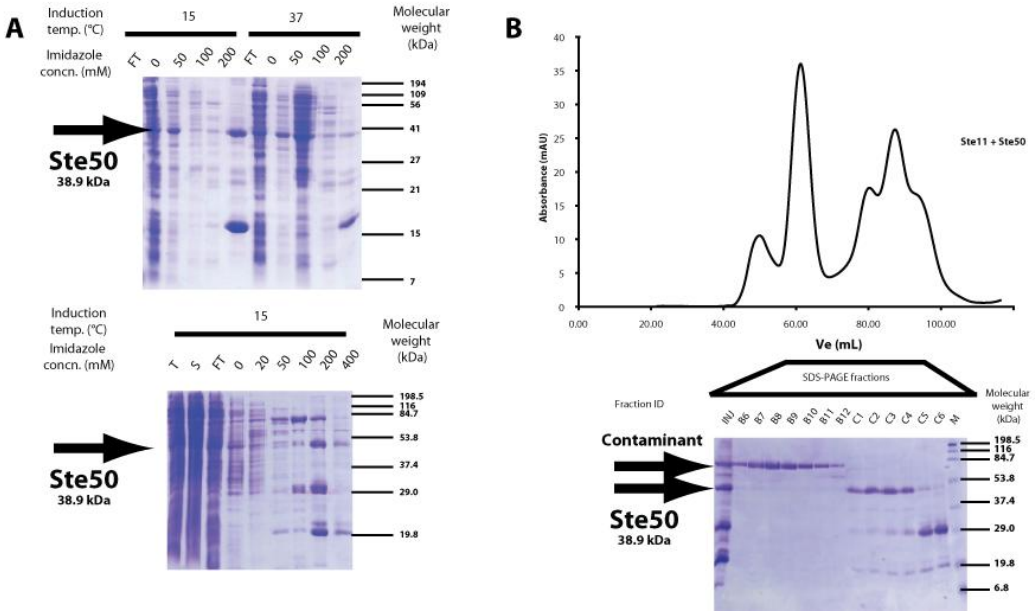

Supplemental Figure 7: Effects of expression using synthetic genes using codon optimization, relative to naturally occurring genes

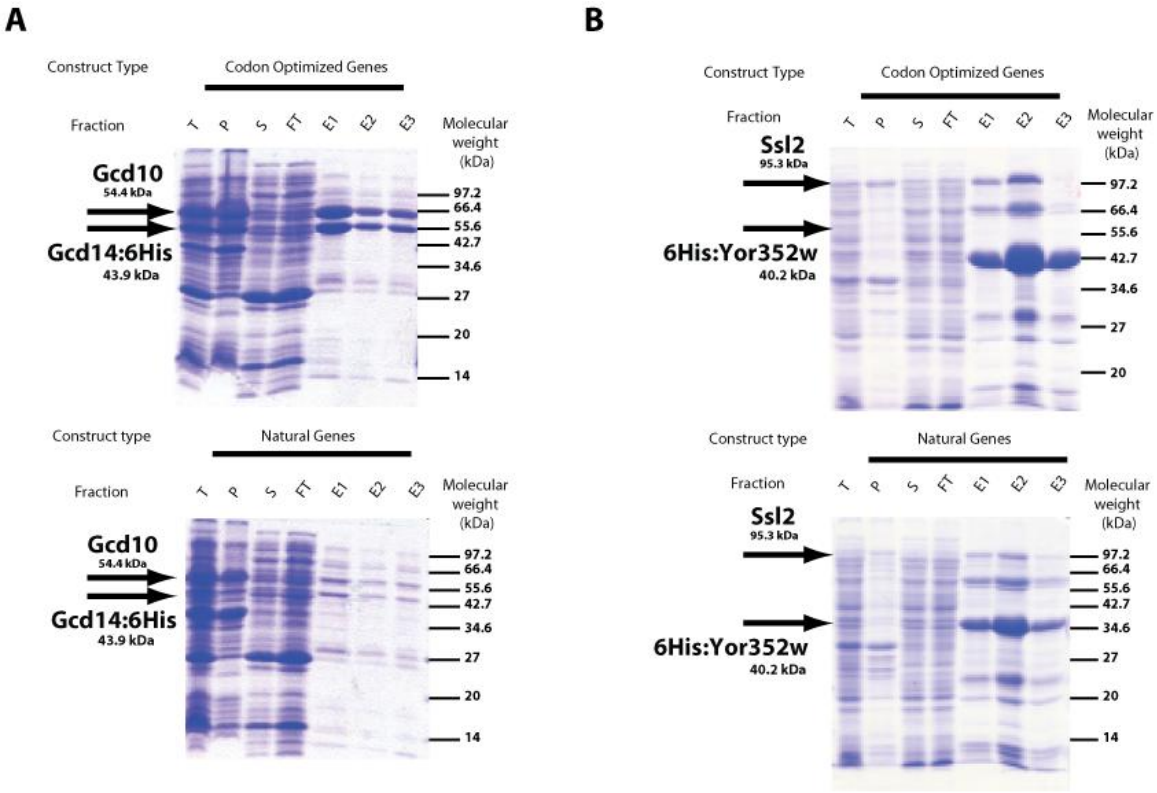

Supplemental Figure Legends

Supplemental Figure 1: Experimental validation of complexes

Experimental validation of the complexes was based on tandem affinity purification. To test the existence of a potential complex *in vivo*, we used several yeast strains; each with expression of the TAP tagged protein from the complex. Tandem affinity purification of TAP tagged proteins was prepared in native conditions, which allows for co-purification of all other proteins forming a complex. In the top left panel of each page, the results from independent purifications of all proteins forming a potential assemble are presented. Proteins from 5 fractions obtained during TAP purification (1; IgG SDS eluate, 2; Calmodulin SDS eluate, 3; IgG eluate, 4; Calmodulin flow, 5; Calmodulin eluate) were separated on 4-12 % gradient SDS-PAGE gels. Proteins were visualized with Coomassie staining. Protein bounds marked with numbers and proteins from the IgG eluate were analyzed with the use of mass spectrometry. Identified proteins were listed below, together with the obtained score. To conclusively validate a complex, all its components should be visible in gel, in a calmodulin eluate fraction, or at least identified by mass spectrometry in an IgG eluate. To check the expression of TAP tagged proteins, their stability and strength of binding to IgG, western blots were prepared. Total proteins from yeast extracts (1) and from the IgG flow-through (2) were separated on 10% SDS-PAGE gels and transferred to a nitrocellulose membrane. Western blots were prepared with the use of PAP antibodies. The results are presented in the top right panel of each page. In order to estimate the size of the complexes, yeast extracts were separated with the use of size exclusion chromatography on a Superdex 200 column in low (150mM) and high (500mM) concentration of NaCl. 30 fractions from each chromatography were collected and spotted on a nitrocellulose membrane. PAP antibodies were used to detect fractions containing the TAP tagged protein. Intensity of spots was calculated and visualized as curves in the bottom panel of each page. The column was calibrated with the use of protein markers. Each experiment corresponds to validation of the complexes indicated at the top of each panel.

Supplemental Figure 2: Expression & Solubility Trials

15% SDS-PAGE of total extract (T) and clarified (S) cell lysates. Each protein was expressed in BL21 Gold (DE3) (Stratagene) or Rosetta2 (DE3) (Novagen) cells at 15°C (indicated by 15), 28°C (28), and 37°C (37). 10 µL of total and soluble fraction were performed by SDS-PAGE and Coomassie blue stain was used for visualizing the gel, as was for Supplemental Figures 2-8. Molecular weight markers and their sizes are indicated at right. Each band adjudged to be of approximate molecular weight concordant with the proteins of interest is indicated by a red asterisk.

Supplemental Figure 3: Paa1-Ptc2 Purification & Complex Reconstitution

Panel A: SDS-PAGE of fractions from Ni^{2+}-NTA chromatography: "FT", flow through, "0", "50", "100", "200" correspond to washes with standard buffer, including imidazole added to the concentration indicated (in mM). Each protein (Paa1, above and Ptc2, below, labelled at left with an arrow to denote the protein of interest) were expressed at both 15°C and 37°C (indicated with bars above the gel). The proteins were soluble at both of these temperatures. Molecular weight markers and their sizes are indicated to the right of all gels. Panel B: Complex Reconstitution between Paa1 and Ptc2 using a Superdex 75 10/30 (GE Healthcare) gel filtration chromatography. Control fractionations of either Paa1, injected alone (grey dotted line) or Ptc2 alone (grey solid line) eluted later than the more excluded Ptc2-Paa1 complex (solid black line). SDS-PAGE of selected fractions from a 96-well fraction collector are shown below the chromatogram (280 nm absorbance). The lanes compare the injected sample (INJ), as well as the peak fractions (D6-E7), demonstrating the presence of both proteins in the shifted peak.

Supplemental Figure 4: Vps27-Hse1 Purification & Complex Reconstitution

Panel A: SDS-PAGE of fractions from Ni^{2+}-NTA chromatography: "FT", flow through, "0", "30", "100", "400" again correspond to the imidazole concentration in mM. Each protein (Vps27, above and Hse1, below, again labelled to the left with an arrow) were expressed at 37°C (indicated as the previous figure). Both proteins were soluble at both of these temperatures. Molecular weight markers and their sizes are

indicated. Panel B: Complex Reconstitution between Vps27 and Hse1 using a Superdex 200 10/30 (GE Healthcare) gel filtration chromatography. Control fractionations of either Hse1, injected alone (grey dotted line) or Vps27 alone (grey solid line) eluted later than the more excluded Vps27-Hse1 complex (solid black line). SDS-PAGE of selected fractions from a 96-well fraction collector are shown below the chromatogram (280 nm absorbance). The samples compare the injected sample (INJ), as well as the peak fractions (D6-E7), demonstrating the presence of both proteins in the shifted peak.

Supplemental Figure 5: Gcd10-Gcd14 Purification & Complex Reconstitution

Panel A: SDS-PAGE of fractions from Ni^{2+}-NTA chromatography: "FT", flow through, "0", "50", "100", "200" correspond to washes with standard buffer, with imidazole added to the concentration indicated (in mM). Each protein (Gcd10, above and Gcd14, below, (labelled as in Supp. Fig. 3), and both were soluble at both of these temperatures. Molecular weight markers and their sizes are indicated at right. Panel B: It was not possible to purify Gcd10 or Gcd14 in a non-aggregated form singly, so cells expressing each of the proteins alone (Gcd10 and Gcd14, as used in panel A), were combined and sonicated together after being resuspended in a buffer containing 1M NaCl and purified using Ni^{2+}-NTA chromatography as in panel A. Fractions containing Gcd10 and Gcd14 were then loaded onto a Superdex S200 10/30 column, yielding a single, symmetrical peak containing both proteins. Estimation of the molecular weight of the complex by comparison with the elution volumes of molecular weight standards ferritin (440 kDa), beta-amylase (200 kDa) and aldolase (158 kDa) (arrowed) indicates that the complex is of approximately 300 kDa.

Supplemental Figure 6: Ste11-Ste50 Purification & Complex Reconstitution

Panel A: SDS-PAGE of fractions from Ni^{2+}-NTA chromatography: "FT", flow through, "0", "50", "100", "200" correspond to washes of with standard buffer, with imidazole added to the concentration indicated (in mM). Each protein (Ste50, above and Ste11, below, labelled at left with an arrow to denote the protein of interest) were expressed at both 15°C and 37°C (indicated with bars above the gel). Ste11 was found to be insoluble at both of these temperatures, however. Molecular weight markers and

their sizes are indicated to the right. Stay tuned for updates on Ste11 expression. Panel B: Sonication of cells expressing Ste11 and Ste50 (as per the Gcd10:Gcd14 complex) did not yield soluble Ste11. The upper band after gel filtration (arrowed), despite having a molecular weight approximately similar to Ste11 was identified as a contaminant from *E. coli*.

Supplemental Figure 7: Effects of expression using synthetic genes using codon optimization relative to naturally occurring genes

SDS-PAGE of fractions from Ni^{2+}-NTA chromatography purifications of co-expressed Gcd10/Gcd14 (Panel A) and Ssl2/Yor352w (Panel B) as synthetic, codon-optimized genes (above), compared to the naturally-occurring yeast DNA sequences (below). Fractions are labelled as follows: “T”, total cells prior to sonication; “P”, pellet post-sonication, “S”; supernatant post-sonication, “FT”; flow through, “E1” & “E2” are specific elutions with buffer including 300 mM imidazole. Note the increased yield when using codon-optimized genes in both cases.

Supplemental Experimental Procedures

Algorithms for the selection of complexes using bioinformatics

We have already described a selection system to rank protein assemblies based on various parameters (Pache and Aloy, 2008), but recapitulate it here. The algorithm is based on the notion that promising target complexes should be small, compact and homogeneous in order to yield successful expression, purification and structure determination. To rank the complexes, biophysical, biochemical and large-scale proteomics data are incorporated in the form of partial scoring functions that we then normalized and combined into a final feasibility score for each complex.

Briefly, the first individual score refers to the average *socio-affinity* index of the complex (Gavin et al., 2006), which quantifies the tendency of two proteins to interact with each other when tagged and to co-purify when yet other proteins are tagged. The higher the average socio-affinity of a complex, the more of its proteins are predicted be in direct contact, which could be used as an indication for the compactness of the complex. We also consider the molecular weight and the total sequence length of the complex components, since larger proteins are usually more difficult to express. We penalize the presence of low complexity regions, internal repeats, coiled coils and intrinsically disordered stretches, since they often result in insoluble proteins that aggregate when over-expressed (Dale et al., 2003).

Information regarding sub-cellular localization (Huh et al., 2003) and abundance (Ghaemmaghami et al., 2003) of individual proteins is also considered, since complex components are expected to be consistent in these terms. Another criterion employed is the level of conservation of a complex across evolution, which we addressed by considering orthologous protein relationships in 83 eukaryotic species (von Mering et al., 2007). We also used binary interactions extracted from yeast two-hybrid screens in combination with the number of isoforms described for each complex to estimate its self-consistency. This is to capture the independence and homogeneity of each complex with respect to the others. For instance, if a complex contains many binary interactions between its own subunits and few with proteins from other complexes, this decreases the probability of missing components in the definition of the complex. Additionally, the fewer isoforms the more invariant the

protein cluster is. Finally, we used cumulative probabilities to normalize each score to the range [0,1], and calculated a global feasibility score as the weighted average of all normalized partial scores. The final score $S(c)$ assigned to each protein complex c is calculated by taking the weighted average of all normalized partial scores $s_i(c)$, ignoring those which are not applicable for the respective protein complex (e.g. the 'Average abundance ratio' when the abundance of none of the proteins in the respective complex could be determined), and multiplying by 100.

Using a weighted average to combine all partial scores makes it possible to give each partial score a particular weight w_i, which allows us to evaluate its importance and to control its impact on the final score:

$$S(c) = 100 \cdot \frac{\sum w_i P_{\sum}(s_i(c) = x)}{\sum w_i}, w_i \in [0,1]$$

$P_{\sum}(s_i(c) = x)$ denotes the cumulative probability that the partial score $s_i(c)$ of the protein complex c is equal to x, used for normalization to take into account the distribution of the respective partial score and calculated by taking the sum of all probabilities $P(s_i(c) = y)$ over all values $y \leq x$ or $y \geq x$, depending on whether higher or lower values are better for the respective ranking criterion:

$$P_{\sum}(s_i(c) = x) = \begin{cases} P(s_i(c) \leq x), \text{better scores are obtained for high } x \text{ values} \\ P(s_i(c) \geq x), \text{better scores are obtained for low } x \text{ values} \end{cases}$$
$$= \begin{cases} \sum_{y \leq x} P(s_i(c) = y), \text{better scores are obtained for high } x \text{ values} \\ \sum_{y \geq x} P(s_i(c) = y), \text{better scores are obtained for low } x \text{ values} \end{cases}$$

Cloning into T7 promoter-based expression systems

Cloning strategy used for single-subunit expression

For the expression and production of single proteins, a cloning strategy to generate C-terminally 6His-tagged proteins was employed. In order to minimize the possibility that errors could be introduced into the primers, to test for the presence of restriction sites in the gene, and to find optimal melting temperatures for primer pairs, a web interface-based script was written. The web interface is part of a basic laboratory information management system (LIMS), which additionally allows the storage of the primers in a structured query language (SQL) database. The software is open source, and freely available: http://plasmidb.sourceforge.net.

PCR reactions were performed with oligonucleotides which encoded either a 5´ *Nco* I or *Nde* I restriction site (the choice of restriction site was determined by the absence of this restriction site in the gene of interest), and a 3´ primer which contains a *Not* I site, followed by a sequence encoding a 6His tag and a stop codon. The oligonucleotides used in this study are listed in Supplemental Table 1. PCR using these primers and *Saccharomyces cerevisiae* S288C genomic DNA as template yielded DNA fragments of the expected size for all of the desired genes, except for Ste11, which we were unable to produce. The resulting PCR products that encoded a 5´ *Nde* I site were cloned into the vector pET9 (Novagen), and those containing *Nco* I sites were cloned into pET28 (Novagen), using standard procedures. Since it was not possible to obtain a PCR product of Ste11, despite numerous attempts with different primers and melting temperatures, the gene encoding Ste11 was ordered as a synthetic gene.

Cloning strategy used for multi-plasmid co-expression

The vector DNA pET-NKIb 3C/LIC (10µg) was digested with *Kpn* I (2-3h at 37°C; NEB) and purified with a QIAquick spin column (Qiagen) according to the

manufacturer's protocol. The linearised vector was treated with T4 DNA Polymerase in the presence of 25 mM dTTP to generate single-strand overhangs. The reaction was incubated at room temperature for 30 min and inactivated by incubating at 75°C for 20 min. Target genes were amplified by PCR using the *Pfu* Turbo polymerase (Stratagene). For the pET-NKIb 3C/LIC the 5'-end of the primers must incorporate the CAGGGACCCGGT sequence upstream the forward PCR primer and the CGAGGAGAAGCCCGGTTA sequence upstream of the reverse primer (which includes a TAA stop codon). For the pET-NKIb LIC without a 6His-tag (no-tag constructs), the sequence GGGCCCGGCGATG must be incorporated in the 5'-end of the primers. A web server enabling the high throughput design of PCR primers was used and is freely available at http://xtal.nki.nl/ccd. The PCR products were purified prior to T4 treatment (QlAquick PCR purification kit by Qiagen); 0.2 pmol of purified PCR DNA was treated with T4 DNA Polymerase in the presence of 25 mM dATP to create the single-strand overhangs. The reaction was incubated at room temperature for 30 min and inactivated by incubation at 75°C for 20 minutes.

Annealing of the vector and insert was achieved by mixing 1 μl pET-NKIb 3C/LIC vector (50ng/μl) with 2 μl insert (0.02 pmol). The reactions were incubated at RT for 5 min, after which 1 μl of 25 mM EDTA was added. Typically, half of the annealing reaction (2µl) is transformed into NovaBlue competent cells (Novagen) and after overnight incubation at 37°C, the annealing and transformation efficiency can be verified. A typical transformation protocol was used (incubation on ice-20 min; heat shock- 30 sec at 42°C; incubation on ice 2 min; addition of 80 μl LB medium to each sample and incubation at 37°C for 1 hour) and transformants are plated on LB agar supplemented with kanamycin (30mg/ml for all his-tag constructs) or ampicillin (100mg/ml; for all no-tag constructs) and incubated at 37°C overnight. Plasmid DNA was extracted from single colonies using a miniprep kit (Qiagen) and restriction digestion was used to verify the presence of the insert of interest.

Cloning strategy used for poly-cistronic expression

For operon constructions, oligonucleotides were designed to amplify coding regions by PCR. Oligonucleotides contained restriction sites selected to be unique in the final plasmid, allowing the simultaneous insertion of both ORFs in the plasmid vector pBS3021. Oligonucleotides contained in addition a Shine-Dalgarno sequence

upstream of the second ORF and a sequence encoding a 6His tag fused in-frame upstream or downstream of one of the two ORFs. PCR fragments were inserted by standard cloning downstream of the T7 promoter of the pBS3021 expression vector. DNA purifications were performed on an EPmotion robot (Eppendorf) using a Macherey-Nagel mini-preparation kit followed by digestion and gel electrophoresis to ascertain the presence of the desired inserts. Inserted fragments were entirely sequenced to confirm the absence of PCR-induced mutations.

Expression testing

Expression testing of individual subunits

The initial objective in this part of the study was to define expression conditions that gave optimal yields of soluble protein for each full-length protein. Therefore, each expression vector under study was initially transformed into both Rosetta pLysS (Novagen) and Gold (Stratagene) in a 24-well block (Corning, Inc.). After incubation overnight in 5 ml per well of 2x Yeast Tryptone (2YT hereafter) medium supplemented with 30 μ g/ml kanamycin at 37° C, this pre-culture was used to inoculate 10 ml per well of similar media as the expression culture, again using 2YT broth supplemented with 30 μ g/ml kanamycin. The volume of the inoculum used was adapted according to its OD_{600} so as to obtain a starting optical density of 0.1 for the expression culture. This culture was incubated until the OD_{600} reached ~1, then was separated into three 1ml aliquots, one for each of the expression temperatures under study: 37ºC, 28ºC and 15ºC. After the addition of IPTG to a final concentration of 0.5 mM, the cells were incubated either for 4 hours at 37ºC, or for 16-18 hrs for the inductions at 28ºC and 15ºC. Cells were harvested by centrifugation of the 24-well block at 5,300 rpm for 1 hour.

The pellets in each well were re-suspended with lysis buffer (20 mM Tris-HCl, pH 7.5, 200 mM NaCl, 5mM β-mercaptoethanol). The 24-well block containing the cell suspension was sonicated with 1 mM benzonase, 4 times for 10 minutes, and then centrifuged at 5,300 rpm for 1 hour. The crude and clarified cell lysates were analyzed using SDS-PAGE (Table 1, column labeled “Single subunit expression” and Supplemental Fig. 1). All proteins except for Ste11 could be produced in a soluble form. Expression from a construct corresponding to Ste11 did

not yield soluble protein, however. An expressed band apparent in purifications at approximately the expected size of Ste11 was in fact identified by mass spectrometry of tryptic digest of this band as polymyxin resistance protein arnA (UniProt accession code; P77398), a common contaminant of purifications originating from *E. coli*.

Expression testing for multi-plasmid co-expression

Small-scale protein expression and solubility screening was carried out for single constructs of full-length proteins, for constructs of individual or combinations of domains as well as for co-expressions of partners. For the transformation of single plasmids, plasmid DNA was transformed into *E. coli* Rosetta2 (DE3) T1R. Single colonies were used for small-scale expression trials in a 24-well 'Deepwell' block (Corning). Each well contained 3ml LB media supplemented with kanamycin 30mg/ml. For the transformation of multiple plasmids to co-express complexes, plasmid DNA of the two partners of interest was transformed into Rosetta2 (DE3) T1R *E. coli* and plated onto LB agar plates supplemented with 30 mg/ml kanamycin and 100 mg/ml ampicillin. Single colonies were used for small-scale expression trials in a 24-well 'Deepwell' block. Each well contained 3 ml LB media supplemented with 30mg/ml kanamycin and 100 mg/ml ampicillin.

The 24-well block was incubated in a shaking incubator at 500 rpm until an OD_{600} of about 0.6-0.8 had been attained, at which point the temperature was reduced to 16°C and the cultures were induced by the addition of IPTG to a final concentration of 1 mM. Incubation was continued for 16-18 hrs and cells were harvested by centrifugation of the Deepwell block at 4,000 rpm for 15 minutes. The pellets in each well were resuspended with lysis buffer (40% sucrose, 50 mM Tris-HCl pH 7.5, 200 mM NaCl, 5mM β-mercaptoethanol, 4mg/ml lysozyme (Novagen), DNAse and PMSF). The 24-well block containing the cell suspension was incubated in a temperature controlled shaking incubator at 300 rpm, for 20 minutes at 10°C and then centrifuged at 4,000 rpm for 15 minutes. The clarified cell lysate was then mixed with 25 μl pre-equilibrated MagneHis Ni-beads (Promega) and incubated at 4°C for 30 minutes. The Magnetight HT96 stand (Novagen) was used to pull down the MagneHis beads. The magnetic beads were washed 3 times with 1 ml wash buffer (lysis buffer supplemented with 20 mM imidazole). Protein elution was performed by

adding 30 μl elution buffer (wash buffer containing 400 mM imidazole) to each sample and eluted fractions were analyzed by SDS-PAGE.

Expression testing for polycistronic co-expression

Proteins were expressed in BL21(DE3) codon+ *E. coli* using auto-induction media(Studier, 2005). Small scale (3 ml) or large scale (100-200 ml) cultures were performed. After overnight incubation at 25°C, cells were harvested. For small-scale cultures, lysis was performed with lysozyme and benzonase. After centrifugation, the supernatant was incubated with Ni-NTA beads for 1h at 4°C. After washing the column with equilibration buffer (50 mM Tris HCl pH7.4, 20 mM imidazole, 300 mM NaCl, 2 mM ß-mercaptoethanol, 0.2 % NP40, 10 % glycerol), proteins were eluted with 500 mM imidazole. For large-scale culture, pellets were washed with PBS and dissolved in 20 ml of equilibration buffer. Cells were lysed using a "Constant Cell Disruption System". After centrifugation, the supernatant was filtered and purified by chromatography on Ni^{2+}-NTA (Akta system, Hitrap Ni^{2+} 1 ml column volume). After washing with equilibration buffer, elution was performed with a linear gradient from 0 to 100% of elution buffer (50 mM Tris HCl pH 7.4, 500 mM imidazole, 300 mM NaCl, 2 mM ß-mercaptoethanol, 0.2% NP40, 10% glycerol). All eluates were analyzed by means of SDS-PAGE.

Complex Formation Trials

Reconstitution of complexes from individually purified partners

We purified Paa1 and Ptc2 to approximate homogeneity using gel filtration and concentrated them individually to 2 mg/ml. The two proteins were combined in a 500 μl reaction mixture (250 μl of each component), and were incubated on ice at 4°C. Gel filtration chromatography illustrated that the proteins co-elute, shifting the peak of Ptc2 by 1.3 ml upon addition of the Paa1 subunit (Supplemental Fig. 3). In a similar manner to the Paa1-Ptc2 complex, both Vps27 and Hse1 could be produced in a soluble form, and the proteins were produced using expression at 37°C henceforth (Supplemental Fig. 4, Panel A). Vps27 and Hse1 proteins were purified to homogeneity using a final gel filtration step. 10nM of each of the proteins were injected separately into an S200 analytical column. Both proteins were then combined and incubated for 30 minutes at 4°C and subjected to gel filtration (Supplemental Fig.

4, Panel B). The complex eluted at 11.03 ml, compared to the individual profiles of Vps27 (11.67 ml) and Hse1 (13.58 ml). Both proteins appear to be in the peak fractions, as judged by SDS-PAGE (Supplemental Fig. 4, lower Panel A). Gcd10 and Gcd14 posed severe problems when purified individually, even from refolded material. Despite being able to obtain both proteins in a relatively soluble form (Supplemental Fig. 5, Panel A), they had a tendency to aggregate as judged by their elution in the void volume of a Superdex S200 column. Eventually, co-sonication of the individually expressed proteins was attempted, which improved the situation considerably. However, it was only when co-sonication was performed in the presence of a high salt buffer (1M NaCl) that an acceptable elution profile was obtained, as has been previously reported (Ozanick et al., 2005) (Supplemental Fig. 5, Panel B). Formation of the complex between Ste11 and Ste50 was prevented by the lack of soluble expression of Ste11 (Supplemental Fig. 6, Panel A, lower) even when co-expressed with Ste50. Ste50 could be produced in a soluble form even when expressed alone, although what appeared to be degradation products were visible (Supplemental Fig. 6, panel A, upper).

Supplemental References

Dale, G.E., Oefner, C., and D'Arcy, A. (2003). The protein as a variable in protein crystallization. J Struct Biol *142*, 88-97.

Gavin, A.C., Aloy, P., Grandi, P., Krause, R., Boesche, M., Marzioch, M., Rau, C., Jensen, L.J., Bastuck, S., Dumpelfeld, B., *et al.* (2006). Proteome survey reveals modularity of the yeast cell machinery. Nature *440*, 631-636.

Ghaemmaghami, S., Huh, W.K., Bower, K., Howson, R.W., Belle, A., Dephoure, N., O'Shea, E.K., and Weissman, J.S. (2003). Global analysis of protein expression in yeast. Nature *425*, 737-741.

Huh, W.K., Falvo, J.V., Gerke, L.C., Carroll, A.S., Howson, R.W., Weissman, J.S., and O'Shea, E.K. (2003). Global analysis of protein localization in budding yeast. Nature *425*, 686-691.

Ozanick, S., Krecic, A., Andersland, J., and Anderson, J.T. (2005). The bipartite structure of the tRNA m1A58 methyltransferase from S. cerevisiae is conserved in humans. RNA *11*, 1281-1290.

Pache, R.A., and Aloy, P. (2008). Incorporating high-throughput proteomics experiments into structural biology pipelines: identification of the low-hanging fruits. Proteomics *8*, 1959-1964.

Studier, F.W. (2005). Protein production by auto-induction in high density shaking cultures. Protein Expr Purif *41*, 207-234.

von Mering, C., Jensen, L.J., Kuhn, M., Chaffron, S., Doerks, T., Kruger, B., Snel, B., and Bork, P. (2007). STRING 7--recent developments in the integration and prediction of protein interactions. Nucleic Acids Res *35*, D358-362.

Supplemental Movies and Spreadsheets

Click here to download Supplemental Movies and Spreadsheets: SupplementaryMaterialOligonucleotides.xls